

Blockade of the checkpoint receptor TIGIT prevents NK cell exhaustion and elicits potent anti-tumor immunity

Qing Zhang^{1,2}, Jiacheng Bi^{2,3}, Xiaodong Zheng², Yongyan Chen², Hua Wang⁴, Wenyong Wu⁴, Zhengguang Wang⁴, Qiang Wu⁴, Hui Peng², Haiming Wei^{1,2}, Rui Sun^{1,2*} and Zhigang Tian^{1,2*}

Checkpoint blockade enhances effector T cell function and has elicited long-term remission in a subset of patients with a broad spectrum of cancers. TIGIT is a checkpoint receptor thought to be involved in mediating T cell exhaustion in tumors; however, the relevance of TIGIT to the dysfunction of natural killer (NK) cells remains poorly understood. Here we found that TIGIT, but not the other checkpoint molecules CTLA-4 and PD-1, was associated with NK cell exhaustion in tumor-bearing mice and patients with colon cancer. Blockade of TIGIT prevented NK cell exhaustion and promoted NK cell-dependent tumor immunity in several tumor-bearing mouse models. Furthermore, blockade of TIGIT resulted in potent tumor-specific T cell immunity in an NK cell-dependent manner, enhanced therapy with antibody to the PD-1 ligand PD-L1 and sustained memory immunity in tumor re-challenge models. This work demonstrates that TIGIT constitutes a previously unappreciated checkpoint in NK cells and that targeting TIGIT alone or in combination with other checkpoint receptors is a promising anti-cancer therapeutic strategy.

Natural killer (NK) cells are essential anti-tumor effector cells^{1,2}. The activity of NK cells is regulated by a repertoire of co-signaling (either co-stimulatory or co-inhibitory) cell-surface receptors that recognize their respective ligand(s) on target cells or antigen-presenting cells. Unlike antigen-triggered T cells, for which co-stimulatory signaling is required for optimal activation, NK cells are not dominated by any single receptor. Instead, the integration of both co-stimulatory signals and co-inhibitory signals determines the responsiveness of NK cells³.

Co-signaling receptors have attracted a great deal of attention due to the success of their being targeted for immunotherapy^{4–6}. For further harnessing of the effector function of anti-tumor immune cells and extension of the current therapeutic benefit of existing co-signaling-based treatments, it is essential to explore the therapeutic potential of the emerging co-signaling receptors⁷. In addition, the immunostimulatory effects of current immunotherapies, such as blockade of the immunological checkpoint receptors CTLA-4 and PD-1, are limited to T cells, due to the expression profile of such molecules. The therapeutic potential of simultaneously activating anti-tumor T cells and NK cells has not been investigated.

The co-inhibitory receptor TIGIT ('T cell immunoglobulin and immunoreceptor tyrosine-based inhibitory motif domain') is expressed on both T cells and NK cells^{8,9}. Multiple groups^{8,10–12} have shown that TIGIT contributes to immunotolerance by inhibiting not only immune responses mediated by T cells^{8,12} but also those mediated by NK cells^{10,11} through binding its ligand, CD155, on antigen-presenting cells or target cells. Notably, blockade of TIGIT can reverse the exhaustion of cytotoxic T lymphocyte (CTL)-mediated anti-tumor immunity and inhibit tumor growth in preclinical tumor models¹³. In addition, TIGIT expression is associated with

tumor progression in tumor-bearing patients^{13,14}. Thus, blockade of TIGIT might be a promising supplement to the current immunological checkpoint-based anti-tumor immunotherapies. However, the mechanisms of action by which such blockade works in boosting anti-tumor immunity have not been fully explored, which is critical for the direction of upcoming clinical trials.

In this study, we found that TIGIT expression on tumor-infiltrating NK cells was associated with tumor progression and was linked to functional exhaustion of NK cells. We found that TIGIT deficiency in NK cells alone was sufficient to delay tumor growth in vivo and that blockade of TIGIT via monoclonal antibodies reversed the exhaustion of anti-tumor NK cells in multiple tumor models and thereafter improved the overall survival of the host. We further demonstrated that blockade of TIGIT directly subverted the exhaustion of tumor-infiltrating NK cells, independently of the adaptive immune system, and that the presence of NK cells was critical for the therapeutic effects of blockade of TIGIT or the PD-1 ligand PD-L1 or combined blockade of both checkpoints. These findings demonstrate that the NK cell-associated TIGIT signaling pathway has a role in tumors' evasion of the immune system and that reversing NK cell exhaustion is critical for the therapeutic effects of anti-tumor immunotherapy based on the blockade of TIGIT.

Results

High TIGIT expression is associated with exhaustion of tumor-infiltrating NK cells. TIGIT expression is upregulated on T cells during tumor progression^{13,15}. Here we found that TIGIT expression was significantly higher on NK cells in intratumoral (IT) regions than on those in peritumoral (PT) regions in patients with colon cancer (Fig. 1a), while TIGIT expression on CD8⁺ T cells in IT

¹Hefei National Laboratory for Physical Sciences at Microscale, University of Science and Technology of China, Hefei, Anhui, China. ²Institute of Immunology and The CAS Key Laboratory of Innate Immunity and Chronic Disease, School of Life Sciences and Medical Center, University of Science and Technology of China, Hefei, Anhui, China. ³Shenzhen Laboratory of Fully Humanized Antibody Engineering, Institute of Biomedicine and Biotechnology, Shenzhen Institutes of Advanced Technology, Chinese Academy of Sciences, Shenzhen, China. ⁴The First Affiliated Hospital of Anhui Medical University, Hefei, Anhui, China. *e-mail: sunr@ustc.edu.cn; tzg@ustc.edu.cn

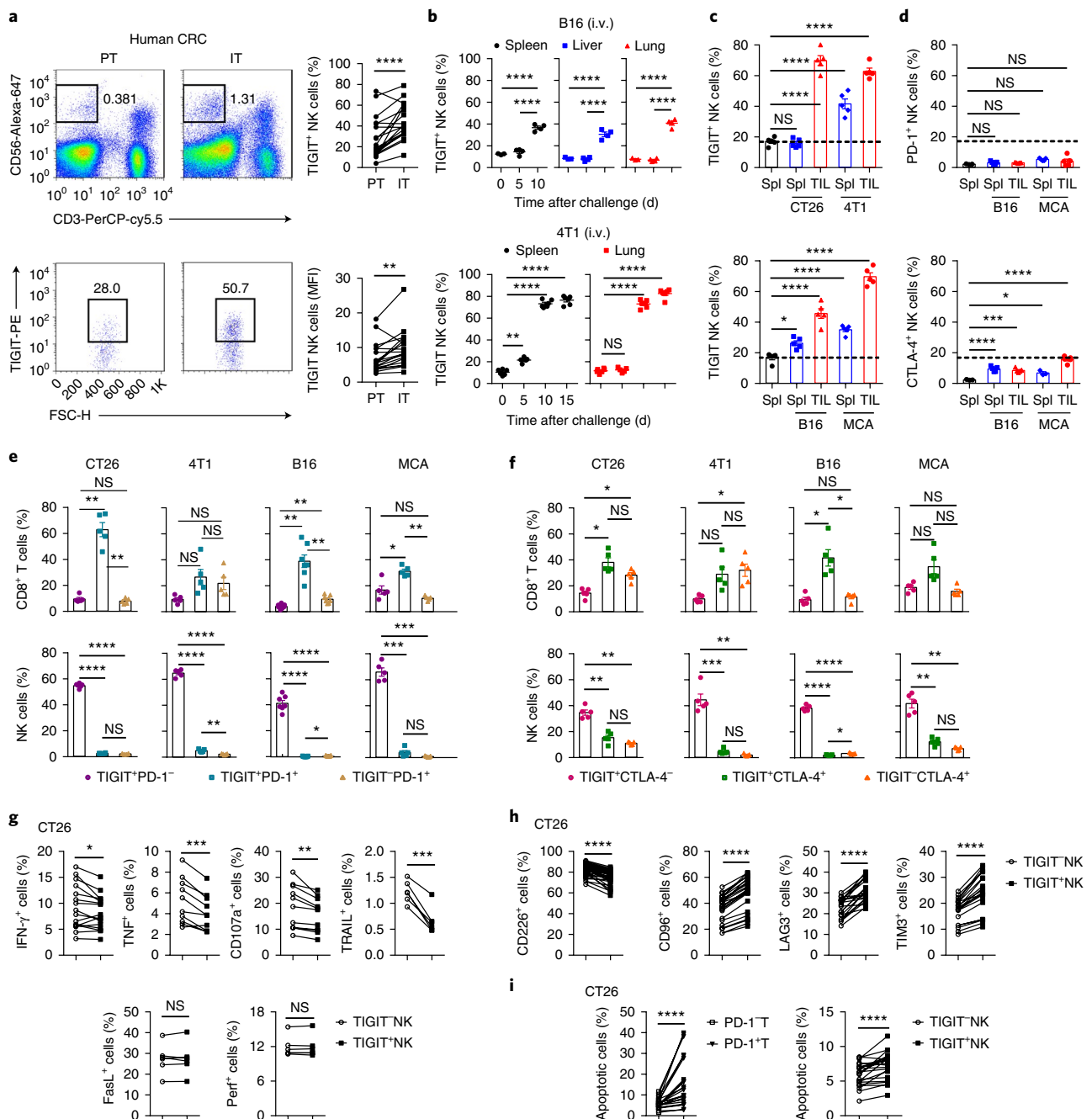


Fig. 1 | TIGIT acts as a newly identified exhaustion marker for tumor-infiltrating NK cells. **a**, Flow cytometry (left) of cells from IT and PT regions (above plots) in patients with CRC ($n=19$), and frequency (top right) and mean fluorescent intensity (MFI) (bottom right) of TIGIT on NK cells (CD45⁺CD3⁻CD56⁺). Numbers adjacent to outlined areas (left) indicate percent CD56⁺CD3⁻ cells (top) or TIGIT⁺ cells (bottom). FSC-H, forward scatter. **b**, Frequency of TIGIT⁺ NK cells in the spleen, liver or lungs (keys) of mice at various times (horizontal axis) after injection (above plots) of 1.5×10^5 B16 cells (top; $n=4$ mice per group) or 4T1 cells (bottom; $n=6$ mice per group) intravenously (i.v.). **c, d**, Frequency of TIGIT⁺ NK cells (**c**) or PD-1⁺ or CTLA-4⁺ NK cells (**d**) among splenocytes (Spl) and tumor-infiltrating lymphocytes (TIL) from mice ($n=5$ per group) given subcutaneous injection of 2×10^5 CT26, 4T1 or B16 cells or 400 μ g MCA (below plots), analyzed when tumor size was around 300 mm³. Dashed lines, average TIGIT expression on splenic NK cells from untreated (control) mice (far left in each plot; $n=5$ (**c**) or $n=3$ (**d**)). **e, f**, Frequency of various subsets (keys) of tumor-infiltrating CD8⁺ T cells (top row) or NK cells (bottom row) from mice ($n=5$ per group) treated as in **c, d** (above plots). **g, h**, Frequency of cells expressing IFN- γ , TNF, CD107a, TRAIL, FasL or perforin (g), or CD226, CD96, LAG3 or TIM3 (h), among tumor-infiltrating TIGIT⁻ NK cells (TIGIT⁻NK) or TIGIT⁺ NK cells (TIGIT⁺NK) (key) from mice ($n=16$ (IFN- γ), 10 (TNF), 11 (CD107a), 6 (TRAIL), 6 (FasL), 6 (perforin), 34 (CD226), 26 (CD96), 21 (LAG3) or 21 (TIM3)) given subcutaneous injection of 2×10^5 CT26 cells, analyzed when tumor size was around 300 mm³. **i**, Frequency of annexin V-positive (apoptotic) cells among PD-1⁻ T cells (PD-1⁻T) or PD-1⁺ T cells (PD-1⁺T) or TIGIT⁻ or TIGIT⁺ NK cells (keys) in TIL populations from mice as in **g, h** ($n=25$ (left) or 23 (right)). Each symbol represents an individual mouse (**b-f**); small horizontal lines (**b**) indicate the mean (\pm s.e.m.); lines (**a-g-i**) connect values for the same patient (**a**) or mouse (**g-i**). NS, not significant ($P > 0.05$); * $P < 0.05$, ** $P < 0.01$, **** $P < 0.001$ and **** $P < 0.0001$ (paired two-tailed t-test (**a-g-i**) or one-way analysis of variance (ANOVA) followed by Tukey's (**b, e, f**) or Dunnett's (**c, d**) multiple-comparisons test (**b-f**)). Data are representative of 19 experiments (**a**) or at least three independent experiments (**b-i**; mean \pm s.e.m. in **c-f**).

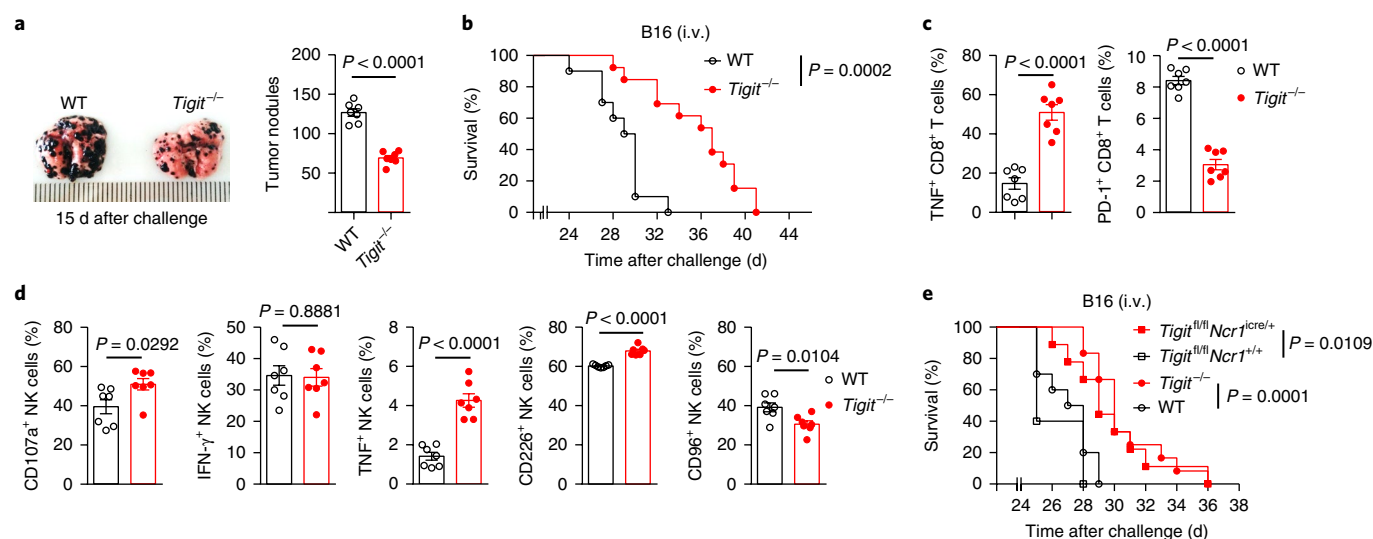


Fig. 2 | TIGIT deficiency inhibits tumor growth and prevents the exhaustion of TILs. a, Images (left) and quantification (right) of tumor nodules on the lungs of wild-type (WT) and *Tigit*^{-/-} mice (key; *n* = 7 per genotype) at day 15 after intravenous injection of 1.5×10^5 B16 cells (challenge). **b**, Survival of wild-type mice (*n* = 10) and *Tigit*^{-/-} mice (*n* = 13) at various times (horizontal axis) after intravenous injection of 5×10^4 B16 cells. **c**, Frequency of cells expressing TNF or PD-1 among tumor-infiltrating CD8⁺ T cells from mice as in **a** (*n* = 7 per genotype), analyzed 15 d after challenge. **d**, Frequency of cells expressing CD107a, IFN- γ , TNF, CD226 or CD96 among tumor-infiltrating NK cells (from mice as in **a** (*n* = 7 per genotype), analyzed 15 d after challenge. **e**, Survival of wild-type mice (*n* = 10), *Tigit*^{-/-} mice (*n* = 12), *Tigit*^{fl/fl}*Ncr1*^{Cre/+} mice (*n* = 9) and *Tigit*^{fl/fl}*Ncr1*^{+/+} mice (*n* = 5) at various times (horizontal axis) after intravenous injection of 5×10^4 B16 cells. Each symbol (**a,c,d**) represents an individual mouse. *P* values, unpaired two-tailed *t*-test (**a,c,d**) or Mantel-Cox test (**b,e**). Data are representative of three independent experiments (mean \pm s.e.m. in **a,c,d**).

regions was not significantly different from that on such cells in PT regions of the same patient ($P > 0.05$ (paired two-tailed *t*-test); Supplementary Fig. 1a). On the basis of those results from human tumors, we investigated TIGIT expression on NK cells in mouse tumor models. In mouse models of pulmonary metastasis of B16 melanoma or 4T1 breast cancer, a high frequency NK cells (Fig. 1b and Supplementary Fig. 1b) and CD8⁺ T cells (Supplementary Fig. 1c) had surface expression of TIGIT in the spleen, liver and lungs (where metastatic tumor nodules grew with time). Such upregulation of TIGIT on tumor-infiltrating NK cells or CD8⁺ T cells was also observed in four mouse models of subcutaneously administered tumors, including CT26 colon cancer, 4T1 breast cancer and B16 melanoma, and fibrosarcoma induced with the chemical carcinogen methylcholanthrene (MCA) (Fig. 1c and Supplementary Fig. 1d,e). We found that although a high frequency of tumor-infiltrating CD8⁺ T cells and CD4⁺ T cells had surface expression of both PD-1 and CTLA-4 (Supplementary Fig. 1f,g), there was only a low frequency of tumor-infiltrating NK cells with surface expression of PD-1 (less than 10%) or CTLA-4 (less than 20%) (Fig. 1d), with their expression being generally well below the TIGIT expression on NK cells from untreated (control) mice. These data indicated that TIGIT was correlated with tumor progression more specifically in NK cells than in other cells in these tumor models. Next, we analyzed TIGIT⁺ subsets among tumor-infiltrating lymphocytes. We found that TIGIT⁺ T cells were mostly PD-1⁺ (Fig. 1e) or CTLA-4⁺ (Fig. 1f and Supplementary Fig. 1h) in all four tumor-bearing models. On the other hand, TIGIT⁺ NK cells were mostly both PD-1⁺ (Fig. 1e) and CTLA-4⁺ (Fig. 1f). This raised the possibility that anti-PD-1 and anti-CTLA-4 therapy might not reverse the dysfunction of NK cells in tumor settings.

We compared the phenotype of TIGIT⁺ NK cell subsets with that of TIGIT⁻ NK cell subsets. We found that a lower frequency of tumor-infiltrating TIGIT⁺ NK cells than TIGIT⁻ NK cells expressed the cytokines IFN- γ and TNF, the lysosome marker CD107a and the cytotoxic molecule TRAIL (Fig. 1g), which suggested that the TIGIT⁺ NK cells possessed reduced effector function and anti-tumor potential.

In addition, a lower frequency of TIGIT⁺ NK cells had surface expression of the activating receptor CD226¹⁶ and higher frequency expressed inhibitory receptors, including CD96¹⁷, LAG3 and TIM3, in CT26 tumor-bearing mice (Fig. 1h) and B16 melanoma-bearing mice (Supplementary Fig. 1i). Meanwhile, modest but significant changes were observed on TIGIT⁺ NK cells for receptors that bind major histocompatibility complex class I molecules, with a greater frequency of cells expressing Ly49A and a lower frequency of cells expressing Ly49C/I, as well as a lower frequency of cells expressing the activating receptor NKG2D and, unexpectedly, the inhibitory receptor NKG2A, for unknown reasons ($P < 0.01$ and $P < 0.001$ (paired two-tailed *t*-test); Supplementary Fig. 1i). Furthermore, a greater frequency of TIGIT⁺ NK cells exhibited apoptosis (Fig. 1i). Thus, similar to PD-1⁺ T cells, TIGIT⁺ NK cells manifested an exhausted phenotype. In addition, the TIGIT ligand CD155 was abundant in human tumors (Supplementary Fig. 2a) and mouse tumors (Supplementary Fig. 2b), whereas the abundance of CD112 was much lower (Supplementary Fig. 2); therefore, CD155 constituted most of the TIGIT ligands in the tumor microenvironment. After binding to the ligand, TIGIT might transduce inhibitory signals to NK cells⁸. Thus, the higher expression of CD155 in the tumor microenvironment might cause more inhibition of TIGIT⁺ cells and lead to the exhaustion of TIGIT⁺ NK cells.

TIGIT deficiency alleviates NK cell exhaustion and slows tumor growth. TIGIT is reported to be involved in the exhaustion of CD8⁺ T cells¹³ and the induction of regulatory T cells¹⁸ in tumor progression. However, the role of TIGIT in NK cell-mediated antitumor responses has not yet been investigated. Here, we intravenously injected B16 melanoma cells into *Tigit*^{-/-} mice (Supplementary Fig. 3a). We found that genetic deficiency in *Tigit* resulted in fewer lung metastases (Fig. 2a) and improved the overall survival of the mice (Fig. 2b) after such injection. We also observed a higher frequency of tumor-infiltrating CD8⁺ T cells expressing TNF and a lower frequency expressing PD-1 (Fig. 2c), and a higher frequency of tumor-infiltrating NK cells expressing CD107a, TNF

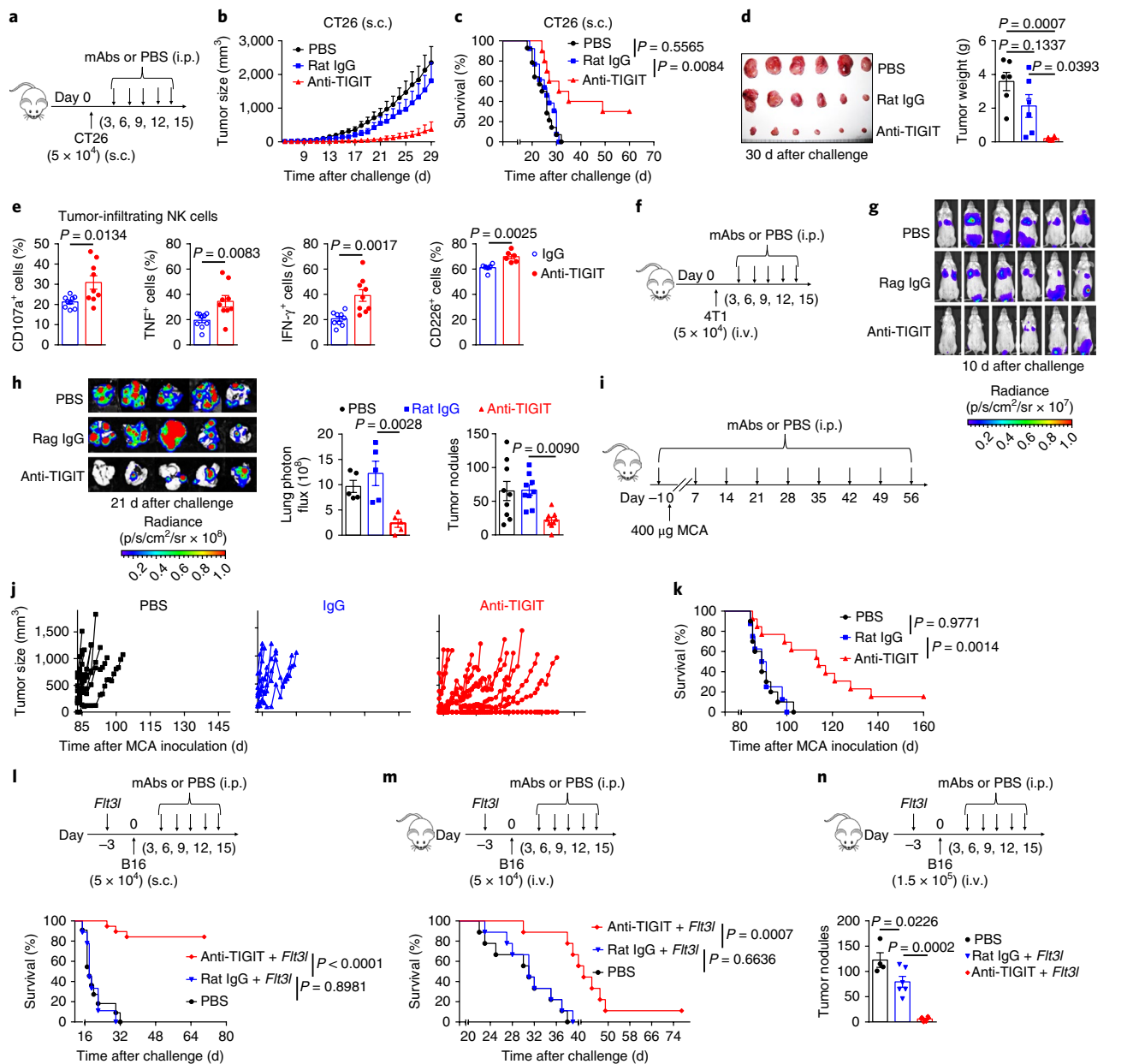


Fig. 3 | Blockade of TIGIT inhibits tumor growth and prevents exhaustion of tumor-infiltrating NK cells. **a**, Experimental protocol for the colon cancer model used in **b–e**: mice were given injection of PBS, mAb to TIGIT or isotype-matched control mAb (rat IgG) intraperitoneally (i.p.) at various times after injection of 5×10^4 CT26 tumor cells subcutaneously (s.c.) on day 0. **b**, Tumor size in mice as in **a** (key; $n=8$ (PBS), $n=6$ (rat IgG) or $n=9$ (anti-TIGIT)) at various times (horizontal axis) after challenge. **c**, Survival of mice as in **a** (key; $n=14$ (PBS), $n=13$ (rat IgG) or $n=10$ (anti-TIGIT)) at various times (horizontal axis) after challenge. **d**, Images of tumors (left) and tumor weight (right) in mice as in **a** (key in **c**; $n=6$ per group) at 30 d after challenge. **e**, Frequency of cells expressing CD107a, TNF, IFN- γ or CD226 among tumor-infiltrating NK cells in mice as in **a** (key; $n=9$ per group), assessed when tumors in mice treated with mAb to TIGIT reached a size of ~ 300 mm 3 . **f**, Experimental protocol for the breast-cancer model used in **g,h**: mice were given injection of PBS or mAbs (as in **a**) intraperitoneally (i.p.) at various times after injection of 5×10^4 4T1 tumor cells intravenously (i.v.) on day 0. **g**, In vivo bioluminescence imaging of pulmonary metastases in mice at 10 d after tumor challenge as in **f**; results (key) are presented as radiance (photons (p) per second per cm 2 of tissue that radiate into a solid angle of one steradian (sr) (p/s/cm 2 /sr)). **h**, In vivo bioluminescence imaging of pulmonary metastases ($n=5$ mice per group) and tumor nodules ($n=9$ mice per group) on the lungs of mice as in **f** at 21 d after challenge, presented as in **g** (key). **i**, Experimental protocol for the MCA-induced fibrosarcoma model used in **j,k**: mice were given injection of PBS ($n=10$ mice), mAb to TIGIT ($n=11$ mice) or isotype-matched control mAb (rat IgG) ($n=8$ mice) intraperitoneally at various times after injection of MCA subcutaneously on day 0. **j**, Tumor growth in mice as in **i** (above plots) at various times (horizontal axis) after injection of MCA. **k**, Survival of mice in mice as in **i** (key) at various times (horizontal axis) after injection of MCA. **l–n**, Experimental protocols (top) for the melanoma models: mice were given injection of plasmid containing *Flt3l* 3 d before (-3) injection of 5×10^4 (**l,m**) or 1.5×10^4 (**n**) B16 tumor cells subcutaneously (**l**) or intravenously (**m,n**) on day 0, then given injection of PBS or mAbs (as in **a**) intraperitoneally at various times after the injection of cells. **l**, Survival of mice ($n=11$ (PBS), $n=9$ (rat IgG) and $n=19$ (anti-TIGIT)) in the subcutaneous model, at various times (horizontal axis) after challenge. **m**, Survival of mice ($n=9$ per group) at various times (horizontal axis) after challenge. **n**, Tumor nodules on the lungs of mice ($n=4$ (PBS), $n=6$ (rat IgG) and $n=6$ (anti-TIGIT)) at 15 d after challenge. Each symbol (**d,e,h,n**) or line (**j**) represents an individual mouse. *P* values, one-way ANOVA followed by Tukey's multiple-comparisons test (**d,h,n**); unpaired two-tailed *t*-test (**e**); Mantel-Cox test (**c,k–m**). Data are representative of three (**a–h,l–n**) or two (**i–k**) independent experiment (mean \pm s.e.m. in **d,e,h,n**).

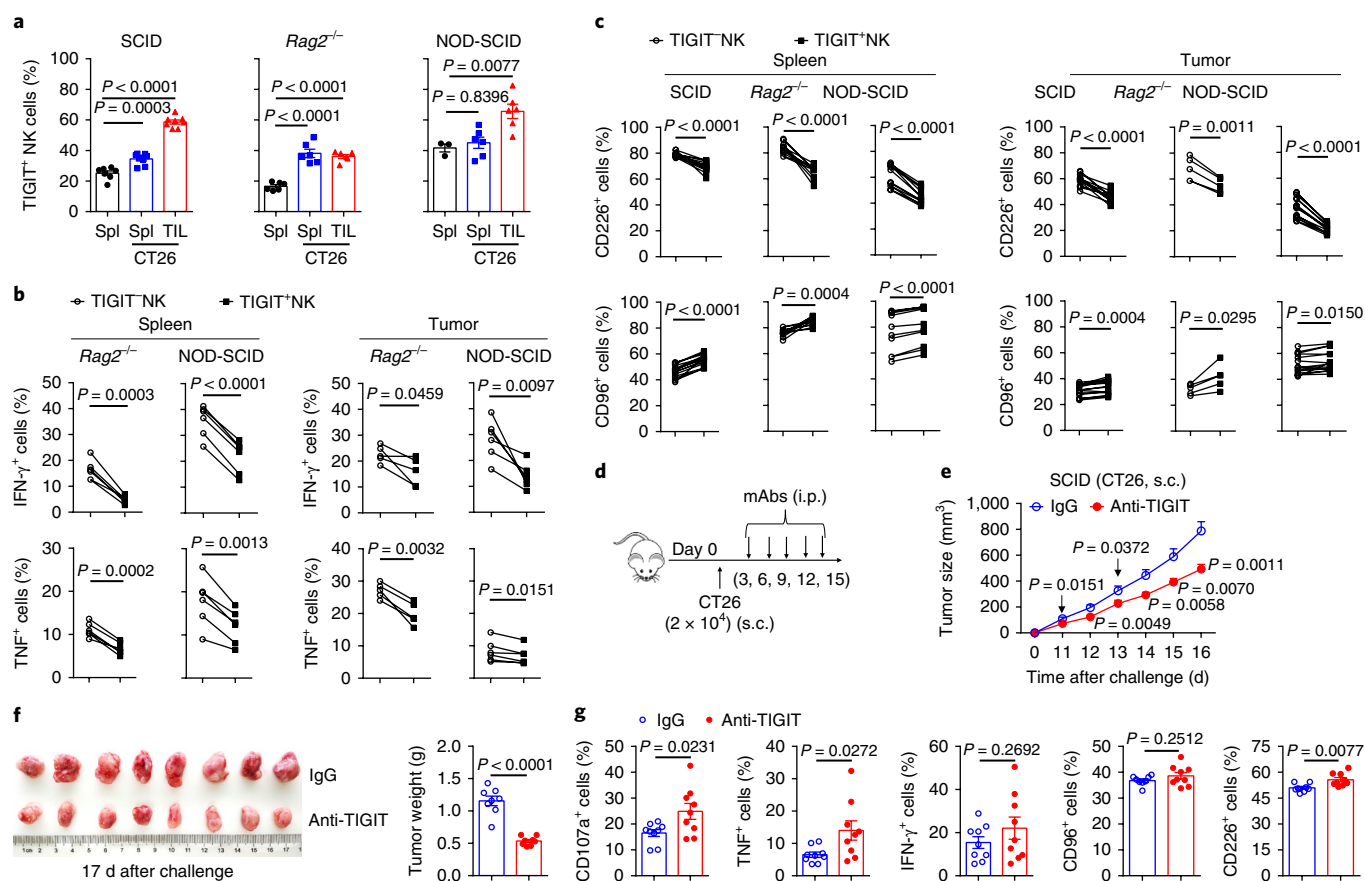


Fig. 4 | Blockade of TIGIT has a protective role in mice with adaptive immunodeficiency. **a**, Frequency of TIGIT⁺ cells among splenic (Spl) or tumor-infiltrating (TIL) NK cells in SCID mice ($n = 7$), $Rag2^{-/-}$ mice ($n = 6$) and NOD-SCID mice ($n = 3$) left untreated (control; far left) or in tumor-bearing SCID mice ($n = 8$), $Rag2^{-/-}$ mice ($n = 6$) and NOD-SCID mice ($n = 6$) after subcutaneous injection of 2×10^5 CT26 cells (below plot). **b**, Frequency of cells expressing IFN- γ or TNF among splenic (Spleen) or tumor-infiltrating (Tumor) TIGIT⁺ or TIGIT⁺ NK cells (key) from tumor-bearing mice as in **a** (spleen, $n = 6$ per group; tumor, $n = 5$ ($Rag2^{-/-}$) or $n = 6$ (NOD-SCID)). **c**, Frequency of cells expressing CD226 or CD96 among splenic or tumor-infiltrating TIGIT⁺ or TIGIT⁺ NK cells from tumor-bearing mice as in **a** (spleen, $n = 15$ (SCID), $n = 11$ ($Rag2^{-/-}$) or $n = 12$ (NOD-SCID); tumor, $n = 15$ (SCID), $n = 5$ ($Rag2^{-/-}$) or $n = 15$ (NOD-SCID)). **d**, Experimental protocol used in **e–g**: SCID mice were given injection of mAb to TIGIT or isotype-matched control mAb (IgG) intraperitoneally at various times after injection of 2×10^4 CT26 tumor cells subcutaneously on day 0. **e**, Tumor size in mice as in **e** ($n = 15$ per group) at various times (horizontal axis) after challenge. **f**, Images of tumors (left) and tumor weight (right) in mice as in **e** ($n = 8$ per group) at 17 d after challenge. **g**, Frequency of cells expressing CD107a, TNF, and IFN- γ CD96, CD226 among tumor-infiltrating NK cells from mice as in **e** ($n = 9$ per group). Each symbol (**a, e–g**) represents an individual mouse; small horizontal lines (**b**) indicate the mean (\pm s.e.m.); lines (**b, c**) connect results for the same mouse. P values, one-way ANOVA followed by Dunnett's multiple-comparisons test (**a**), paired two-tailed t -test (**b, c**), multiple t -tests (**e**) or unpaired two-tailed t -test (**f, g**). Data are representative of at least three independent experiments (mean \pm s.e.m. in **a, e–g**).

and CD226 and a lower frequency expressing CD96 (Fig. 2d), in $Tigit^{-/-}$ mice than in wild-type mice with B16 melanoma metastases. Furthermore, we bred $Tigit^{fl/fl}$ mice with $Ncr1^{iCre/+}$ mice to effect deletion of TIGIT specifically in NK cells in the $Tigit^{fl/fl}Ncr1^{iCre/+}$ offspring. We observed that NK cell-specific deficiency in TIGIT (in $Tigit^{fl/fl}Ncr1^{iCre/+}$ mice; Supplementary Fig. 3a) resulted in significantly prolonged survival of mice relative to that of $Tigit^{fl/fl}Ncr1^{+/+}$ mice or wild-type mice (Fig. 2e), similar to results obtained for $Tigit^{-/-}$ mice. NK cell-specific deficiency in TIGIT also led to a greater frequency of NK cells expressing CD226 and a lower frequency of NK cells expressing CD96 (Supplementary Fig. 3b), which indicated that TIGIT might directly mediate the exhaustion of tumor-infiltrating NK cells. NK cell-specific deficiency in TIGIT resulted in a lower frequency of on tumor-infiltrating CD8⁺ T cells expressing TIGIT and the receptor TIM3 (Supplementary Fig. 3c), which suggested that NK cells expressing TIGIT might also indirectly contribute to the exhaustion of CD8⁺ T cells. Thus, TIGIT expression on NK cells had a non-redundant effect on the impairment of anti-tumor responses.

Blockade of TIGIT prevents NK cell exhaustion in tumor-bearing mice. In order to assess the effects of the blockade of TIGIT on NK cell function in tumor-bearing mice, we treated the mice with monoclonal antibody (mAb) to TIGIT in the settings of colon tumors (Fig. 3a–e), breast tumors (Fig. 3f–h) and chemically induced fibrosarcomas (Fig. 3i–k). In CT26 tumor-bearing mice (Fig. 3a), we found that tumor growth was inhibited by blockade of TIGIT, as shown by lower tumor volume (Fig. 3b) and improved overall mouse survival (Fig. 3c). We also detected a smaller tumor mass 30 d after challenge (Fig. 3d), as well as a higher frequency of tumor-infiltrating NK cells expressing CD107a, TNF, IFN- γ and CD226, in mice treated with mAb to TIGIT than in mice treated with the control antibody IgG (Fig. 3e). These data indicated that blockade of TIGIT reversed the exhaustion of tumor-infiltrating NK cells. The therapeutic effects were accompanied by a higher frequency of tumor-infiltrating CD8⁺ T cells with surface expression of CD107a, TNF and IFN- γ (Supplementary Fig. 4a), which indicated that treatment with antibody to TIGIT (anti-TIGIT) also reversed CTL exhaustion. In line with those findings, in the 4T1-pulmonary

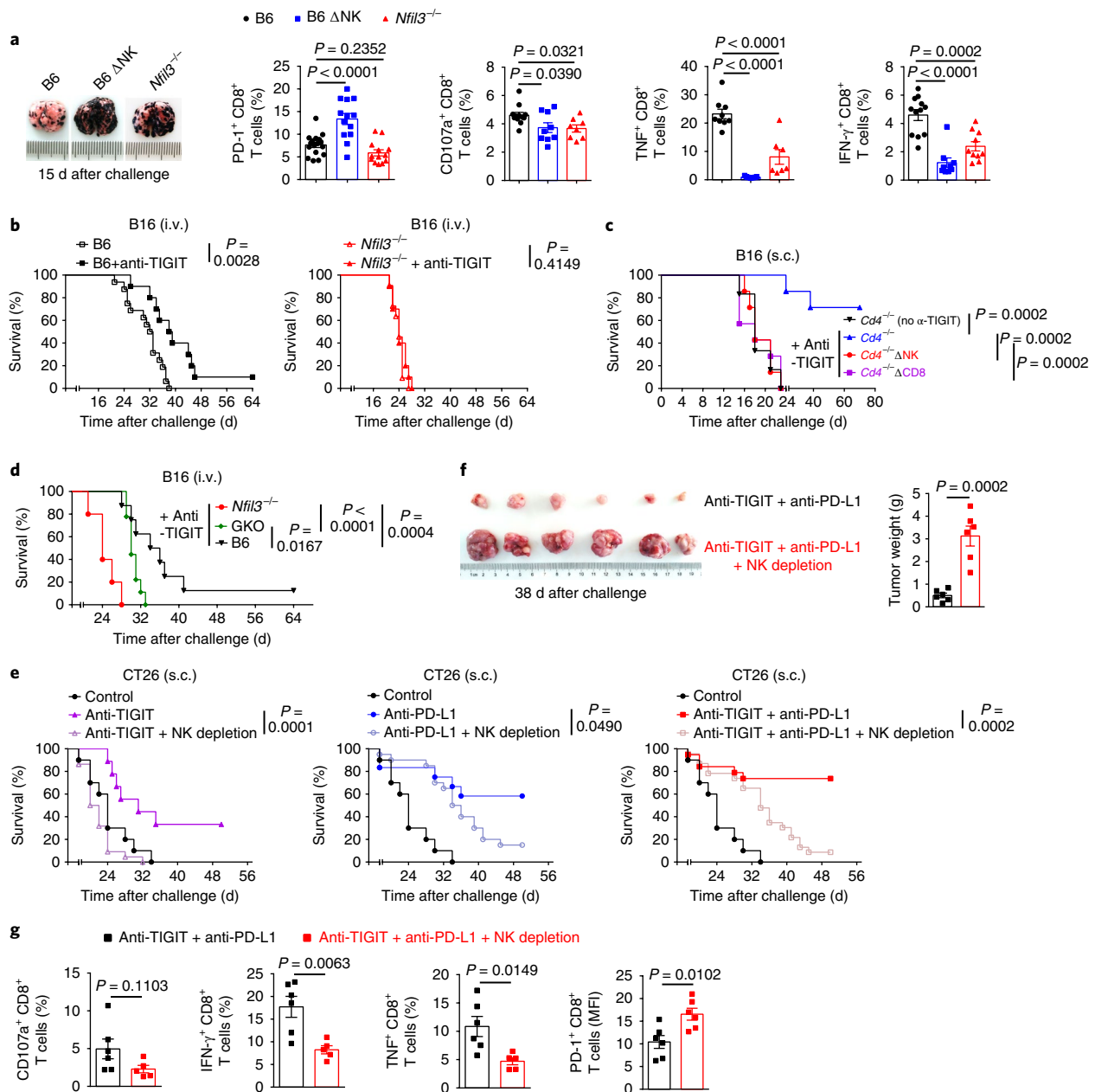


Fig. 5 | NK cells are critical for the anti-tumor efficacy of blockade of TIGIT. a, Images of lungs (far left) from mice given intravenous injection of B16 tumor cells (the B16 pulmonary metastasis model) without deletion of NK cells (B6) or with deletion of NK cells via treatment with anti-NK1.1 (B6 Δ NK) or via knockout of *Nfil3* (*Nfil3*^{-/-}), and frequency of cells expressing PD-1, CD107a, TNF or IFN- γ among tumor-infiltrating CD8⁺ T cells in such mice (middle and right) (PD-1: $n=15$ mice (B6), $n=13$ mice (B6 Δ NK) or $n=13$ mice (*Nfil3*^{-/-}); CD107a: $n=12$, 9 or 8 mice, respectively; TNF: ($n=9$, 9 or 7 mice, respectively); IFN- γ : $n=12$, 9 or 10 mice, respectively). **b**, Survival of B6 mice (left) and *Nfil3*^{-/-} mice (right) as in Fig. 3m, therapeutically treated with mAb to TIGIT ($n=10$ (B6) or $n=10$ (*Nfil3*^{-/-})) or not ($n=16$ (B6) or $n=11$ (*Nfil3*^{-/-})) (key). **c**, Survival of *Cd4*^{-/-} mice treated with anti-TIGIT or not (*Cd4*^{-/-} (no α -TIGIT)) ($n=7$ per group), all assessed at various times (horizontal axis) after subcutaneous injection of B16 tumor cells (the B16 subcutaneous melanoma model, as in Fig. 3l), without deletion of cells (*Cd4*^{-/-}) or with treatment with anti-NK1.1 for the deletion of NK cells (*Cd4*^{-/-} Δ NK) or with mAb to CD8 for the deletion of CD8⁺ T cells (*Cd4*^{-/-} Δ CD8). **d**, Survival of *Nfil3*^{-/-} mice ($n=5$), IFN- γ -deficient (GKO) mice ($n=9$) and B6 mice ($n=8$) (key) as in Fig. 3m, treated with anti-TIGIT, assessed at various times (horizontal axis) after intravenous injection of B16 tumor cells. **e**, Survival of mice given subcutaneous injection of CT26 colon cancer cells alone (Control) ($n=10$) or also treated with anti-TIGIT ($n=9$) or anti-TIGIT plus depletion of NK cells (NK depletion) ($n=22$) (left), with anti-PD-L1 ($n=12$) or anti-PD-L1 plus depletion of NK cells ($n=20$) (middle), or with anti-TIGIT plus anti-PD-L1 ($n=19$) or anti-TIGIT plus anti-PD-L1 plus depletion of NK cells ($n=23$), assessed at various times (horizontal axis) after challenge. **f**, Images of tumors (left) and tumor weight (right) of mice ($n=6$ per group) given subcutaneous injection of CT26 colon cancer cells and treated with anti-TIGIT plus anti-PD-L1 or anti-TIGIT plus anti-PD-L1 plus depletion of NK cells, assessed at 38 d at challenge. **g**, Frequency of cells expressing CD107a, IFN- γ or TNF and mean fluorescent intensity of PD-1-expressing cells among tumor-infiltrating CD8⁺ T cells in mice as in **f** ($n=6$ per group). Each symbol (**a**, **f**, **g**) represents an individual mouse. *P* values, one-way ANOVA followed by Dunnett's multiple comparisons test (**a**), Mantel-Cox test (**b**–**e**) or unpaired two-tailed *t*-test (**f**, **g**). Data are representative of at least three independent experiments (mean \pm s.e.m. in **a**, **f**, **g**).

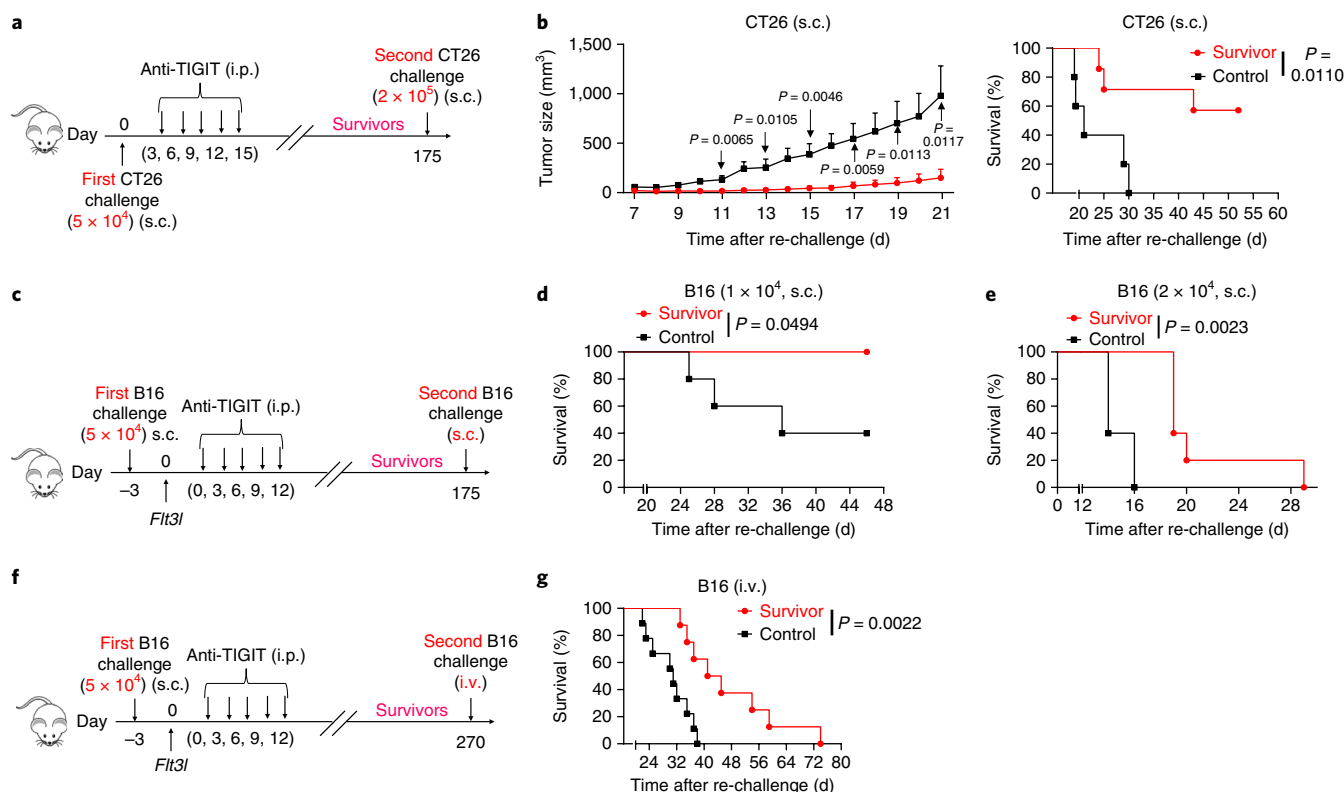


Fig. 6 | Blockade of TIGIT improves memory response to tumor re-challenge. **a**, Experimental protocol for **b**: mice were given injection of anti-TIGIT intraperitoneally at various times after initial injection of 5×10^4 CT26 tumor cells subcutaneously on day 0, then tumor-free mice (Survivors) were re-challenged by injection of 2×10^5 CT26 tumor cells subcutaneously. **b**, Tumor size (left) and survival (right) of mice as in **a** (Survivor) ($n = 7$) and age-matched tumor-naïve mice (Control) ($n = 5$). **c, f**, Experimental protocol for **d, e, g**: mice were given injection of anti-TIGIT intraperitoneally at various times after initial injection of 5×10^4 B16 tumor cells subcutaneously 3 d before treatment with plasmid containing *Flt3l*, then tumor-free mice (Survivors) were re-challenged by injection of B16 tumor cells subcutaneously (**c**) or intravenously (**f**). **d, e**, Survival of mice ($n = 5$ per group) re-challenged subcutaneously as in **c** with 1×10^4 B16 cells (**d**) or 2×10^4 B16 cells (**e**) (Survivor) and age-matched tumor-naïve mice (Control). **g**, Survival of mice re-challenged intravenously as in **f** (Survivor) ($n = 8$) and age-matched tumor-naïve mice (Control) ($n = 9$). P values, multiple t-tests (**b** (left)) or Mantel-Cox test (**b** (right), **d, e, g**). Data are representative of at least two independent experiments (mean \pm s.e.m. in **b** (left)).

metastasis model (Fig. 3f), treatment with anti-TIGIT reduced tumor metastasis with blockade of TIGIT at various time points after tumor inoculation (Fig. 3g,h). In the MCA-induced fibrosarcoma model, in which a mutagenic chemical induced spontaneous tumors, with considerable variation between individual mice in tumor growth (Fig. 3i), treatment with anti-TIGIT delayed tumor growth and prolonged overall mouse survival (Fig. 3j,k). Thus, in addition to its effects on CTLs, blockade of TIGIT prevented the exhaustion of NK cells in tumor-bearing mice.

B16 melanoma is well recognized as an aggressive tumor with poor immunogenicity^{19,20}, and it was poorly controlled with any monotherapy such as anti-TIGIT (Supplementary Fig. 4b,c) or blockade of CTLA-4 or PD-1^{21–25}. The cytokine Flt3L has been used extensively to improve immunotherapeutic efficacy through its action as potent stimulator of dendritic cells^{26–29}, and when combined with blockade of CTLA4 or PD-1, it accelerates the rejection of tumors^{23,24}. Since Flt3L can also stimulate the population expansion and function of NK cells^{30,31}, we hydrodynamically injected plasmid containing the gene encoding mouse Flt3L (*Flt3l*) into mice to overexpress mouse Flt3L in vivo and found that such delivery of *Flt3l* alone resulted in a high concentration of Flt3L in serum (Supplementary Fig. 5a), along with a high frequency of functional NK cells as well as dendritic cells in blood and immune-system organs (Supplementary Fig. 5a–c). When used in conjunction with delivery of *Flt3l*, blockade of TIGIT substantially extended the

survival of B16 tumor-bearing mice (after subcutaneous injection of B16 cells), but delivery of *Flt3l* alone showed no such benefit (Fig. 3l). That therapeutic effect on overall survival was further confirmed in a B16 pulmonary metastasis model (with intravenous injection of B16 cells) (Fig. 3m), and its beneficial effect on tumor metastases was also confirmed, even in mice given injection of a large number of tumor B16 cells (Fig. 3n). Also, we found more infiltration of activated (CD69⁺) NK cells into tumors in the group in which TIGIT was blocked (Supplementary Fig. 5d), which indicated that blockade of TIGIT enhanced the infiltration of activated NK cells into tumors. Collectively, these results demonstrated that therapeutically blocking TIGIT in vivo through the use of a mAb might enhance anti-tumor immunity by reversing the exhaustion of tumor-infiltrating NK cells, directed against strongly or weakly immunogenic tumors, established tumors or metastasis.

Blockade of TIGIT prevents NK cell exhaustion in the absence of adaptive immunity.

In order to explore whether blockade of TIGIT could also enhance anti-tumor immunity in mice in the absence of the adaptive immune system, we assessed the expression and function of TIGIT in immunodeficient *Rag2*^{-/-} mice, mice of the T cell-deficient severe combined immunodeficiency (SCID) strain, and mice of the non-obese diabetic (NOD)-SCID strain, all after injection of CT26 cells. We found that a greater frequency of NK cells had surface expression of TIGIT, in both the spleen and

CT26 tumors, for all three groups of mice (Fig. 4a). We also found that a lower frequency of TIGIT⁺ NK cells than TIGIT⁻ NK cells expressed IFN- γ or TNF (Fig. 4b) or CD226 (Fig. 4c) and a greater frequency of TIGIT⁺ NK cells than TIGIT⁻ NK cells expressed the inhibitory receptor CD96 (Fig. 4c) in both the spleen and tumors. Next, we treated CT26 tumor-bearing *Rag2*^{-/-}, SCID and NOD-SCID mice with mAb to TIGIT (Fig. 4d). We found that treatment with anti-TIGIT slowed tumor growth (Fig. 4e) and reduced tumor mass in T cell-deficient SCID mice (Fig. 4f). Following blockade of TIGIT, tumor-infiltrating NK cells showed improved function in SCID mice, as indicated by the increased frequency of such cells expressing CD107a, TNF, IFN- γ or CD226 (Fig. 4g). Since TIGIT was expressed mainly only on T cells and NK cells, these exhaustion-reversing effects of anti-TIGIT in T cell-deficient SCID mice suggested that the effect was achieved directly via NK cells. The therapeutic effect of blockade of TIGIT was further confirmed in *Rag2*^{-/-} mice and even NOD-SCID mice, a mouse model with functional impairment of NK cells (Supplementary Fig. 6). These data indicated that reversal of NK cell exhaustion and improved tumor responses could be achieved with blockade of TIGIT even in the absence of functional adaptive immune cells.

Blockade of TIGIT improves adaptive immunity in an NK cell-dependent manner. Both NK cells and CTLs expressed TIGIT (Fig. 1a–c and Supplementary Fig. 1a–h). We attempted to delineate the effect of NK cells on T cells in the setting of the blockade of TIGIT. For this, we deleted NK cells either by using mice deficient in the gene encoding the transcription factor E4BP4 (*Nfil3*-knockout mice), which totally lack conventional NK cells, or by treating mice with antibody to the NK cell receptor NK1.1. In the B16 pulmonary metastasis model (intravenous injection of B16 cells), we found that the deletion of NK cells led to more lung metastasis, along with a greater frequency of CD8⁺ T cells expressing PD-1 and a lower frequency of CD8⁺ T cells expressing CD107a, IFN- γ or TNF (Fig. 5a). These findings indicated that NK cells were normally involved in the control of B16 metastasis and also potentially enhanced the function of CD8⁺ T cells and/or prevented their exhaustion. Moreover, we found that NK cell deficiency abolished the therapeutic effect of blockade of TIGIT even in the presence of TIGIT-expressing CD8⁺ T cells (Fig. 5b). This suggested CTLs were more severely exhausted in the absence of NK cells, even under blockade of TIGIT. Since CD4⁺ T cells (such as regulatory T cells) also expressed TIGIT, we sought to determine whether the therapeutic effect of blockade of TIGIT was influenced by these cells. Thus, we set up a study with mice deficient in the T cell-specific co-receptor CD4 (*Cd4*^{-/-} mice). In NK cell-sufficient *Cd4*^{-/-} mice challenged with B16 melanoma subcutaneously, blockade of TIGIT retained the anti-tumor effect (Fig. 5c), which suggested that CD4⁺ T cells were not critical in our setting. However, with the removal of NK cells, the effect was abolished even in the presence of CD8⁺ T cells, and this was comparable to the removal of CD8⁺ T cells (Fig. 5c), which indicated that blockade of TIGIT on CD8⁺ T cells alone was insufficient to mount effective anti-tumor immunity in the absence of NK cells. These data demonstrated that during blockade of TIGIT and enhancement of tumor immunity, NK cells, at least in part, had a critical role in supporting CD8⁺ T cells. We also found that IFN- γ was important, at least partially, for the anti-tumor function of NK cells, because blockade of TIGIT did not exert any anti-tumor effect in IFN- γ -deficient mice (Fig. 5d). These results indicated that NK cells not only exerted a direct anti-tumor effect but also assisted the function of CD8⁺ T cells, in the setting of blockade of TIGIT.

To confirm the anti-tumor role of NK cells during checkpoint blockade with anti-TIGIT or anti-PD-L1, we compared their therapeutic efficacy with or without deletion of NK cells. We found that the therapeutic effects of anti-TIGIT, anti-PD-L1 or anti-TIGIT plus anti-PD-L1 depended on the presence of NK cells (Fig. 5e,f),

as indicated by overall survival (Fig. 5e) and tumor weight (Fig. 5f). The absence of NK cells also resulted in a lower frequency of tumor-infiltrating CD8⁺ T cells expressing IFN- γ or TNF, as well as an elevated frequency of tumor-infiltrating CD8⁺ T cells expressing PD-1 (Fig. 5g), in mice receiving the combinational therapy. Thus, these data highlight the importance of NK cells not only in therapy involving blockade of TIGIT or PD-L1 but also in combination therapy targeting both TIGIT and PD-L1.

Blockade of TIGIT elicits a potent antitumor memory response.

The results reported above showed that blockade of TIGIT elicited potent primary adaptive anti-tumor immunity in an NK cell-dependent manner. Next we investigated whether mice that had survived tumor challenge following blockade of TIGIT had anamnestic responses to tumor re-challenge. CT26 tumor-bearing mice were initially treated with mAb to TIGIT and were subsequently given re-injection of a fourfold amount of CT26 cells on day 175 after the first tumor inoculation and in the absence of any further treatment (Fig. 6a). We observed that tumor growth was inhibited and mouse survival was increased, relative to that of tumor-naïve mice (Fig. 6b). Similar results were obtained in B16 tumor-bearing mice (Fig. 6c) with low and high doses of subcutaneous tumor re-challenge (Fig. 6d,e). In addition, these mice retained recall responses to intravenous tumor re-challenge on day 270 after the first challenge (Fig. 6f,g). Together these results demonstrated that anti-TIGIT immunotherapy alone elicited anti-tumor immune memory.

Discussion

Immunological checkpoint-based anti-tumor therapy has attracted extensive attention⁶. It is thought that blockade of PD-L1, PD-1 and CTLA-4 boosts effector T cell-mediated anti-tumor immunity. How to extend the clinical benefits to the majority of patients with cancer and exploring novel therapeutic targets have been key focuses of this area. Like anti-tumor CTLs, NK cells are essential anti-tumor effector cells that are also functionally tolerant in tumor microenvironments. However, limited preclinical studies have explored the potential of boosting NK cell-mediated anti-tumor immunity. TIGIT is a cell-surface inhibitory receptor. Unlike PD-1 and CTLA-4, TIGIT is expressed by both T cells and NK cells⁸. Emerging studies have shown that blockade of TIGIT might be a potential supplement for existing immunotherapies^{9,13,14,32,33}. However, the mechanisms of action of the blockade of TIGIT are not fully understood. In the current study, we investigated the role of TIGIT in the regulation of NK cell-mediated anti-tumor immunity and the importance of NK cells in the therapeutic efficacy of tumor immunotherapy based on blockade of TIGIT and PD-L1. We found that TIGIT-expressing tumor-infiltrating NK cells were associated with the functional exhaustion of tumor-infiltrating NK cells and tumor progression in mouse tumors. TIGIT deficiency in NK cells alone significantly inhibited tumor growth in vivo. Blockade of TIGIT reversed the exhaustion of NK cells and enhanced NK cell-mediated anti-tumor immunity. Thus, NK cells are critical for the therapeutic effects of the blockade of TIGIT. This suggests that the presence of NK cells and the level of TIGIT expression on NK cells might be critical for the clinical outcome of TIGIT-based immunotherapy.

In our models, PD-1 and CTLA-4 were expressed mainly by tumor-infiltrating T cells and were barely expressed by tumor-infiltrating NK cells, which suggested that blocking PD-1 and CTLA-4 might affect mainly T cells, while NK cells would remain functionally exhausted. Moreover, both NK cells and T cells infiltrating tumors had high expression of TIGIT, which indicated that blockade of TIGIT, as a monotherapy, might be superior in concurrently reversing the exhaustion of both T cells and NK cells, while the single blockade of other molecules (CTLA-4, PD-1 or KIR) can recover the function of only one cell type at a time³⁴. Our data also demonstrated,

for the first time, to our knowledge, that the presence of NK cells was critical for the therapeutic effects of blockade of TIGIT. A published study has reported that depletion of CD8⁺ cells, as well as blocking CD226, diminishes the therapeutic effects of the blockade of TIGIT¹³. Here, we found that the absence of NK cells diminished the therapeutic effects of the blockade of TIGIT, and that blockade of TIGIT directly reversed the exhaustion of tumor-infiltrating NK cells independently of T cells, indicative of a critical role for NK cells in the therapeutic effects of the blockade of TIGIT. Together these findings suggest that the presence of NK cells might be critical for the clinical outcome of TIGIT-based immunotherapy. Moreover, we showed that blockade of PD-L1 also depended on NK cells. Given that NK cells enhanced the function of CD8⁺ T cells and/or prevented their exhaustion, the CD8⁺ T cell–reinvigorating potential of the blockade of PD-L1 might be compromised in the absence of NK cells. This might explain the NK cell–dependent effects of anti-PD-L1 we observed, although we cannot exclude the possibility of direct cytotoxic effects of NK cells in this context.

A published study has shown that dual blockade of PD-L1 and TIGIT results in a secondary response to tumor re-challenge¹³. However, the contribution of NK cells in this context has not been investigated. Here, our data showed that NK cells normally acted to maintain the anti-tumor effector function of CD8⁺ T cells, which would indicate a helper function of NK cells in CTL immunity^{35,36}. In line with that, enhancing NK cell function by NK cell–specific deficiency in TIGIT or blockade of TIGIT might provide additional help in boosting CD8⁺ T cell–mediated primary immunity and possibly in eliciting potent T cell–mediated memory response to tumor re-challenge, as shown in our study. Nevertheless, the mechanisms used by NK cells in the induction of memory responses after blockade of TIGIT still need further investigation. In summary, our findings support the notion that blockade of TIGIT enhances host anti-tumor immunity in a non-redundant NK cell–dependent manner and that the presence of NK cells might be critical for the therapeutic effects of certain immunotherapies.

Methods

Methods, including statements of data availability and any associated accession codes and references, are available at <https://doi.org/10.1038/s41590-018-0132-0>.

Received: 21 April 2017; Accepted: 13 April 2018;
Published online: 18 June 2018

References

- Lanier, L. L. NK cell recognition. *Annu. Rev. Immunol.* **23**, 225–274 (2005).
- Zhang, Q. F. et al. Liver-infiltrating CD11b⁺CD27[−] NK subsets account for NK-cell dysfunction in patients with hepatocellular carcinoma and are associated with tumor progression. *Cell. Mol. Immunol.* **14**, 819–829 (2017).
- Long, E. O., Kim, H. S., Liu, D., Peterson, M. E. & Rajagopalan, S. Controlling natural killer cell responses: integration of signals for activation and inhibition. *Annu. Rev. Immunol.* **31**, 227–258 (2013).
- Chen, L. & Flies, D. B. Molecular mechanisms of T cell co-stimulation and co-inhibition. *Nat. Rev. Immunol.* **13**, 227–242 (2013).
- Pardoll, D. M. The blockade of immune checkpoints in cancer immunotherapy. *Nat. Rev. Cancer* **12**, 252–264 (2012).
- Zou, W., Wolchok, J. D. & Chen, L. PD-L1 (B7-H1) and PD-1 pathway blockade for cancer therapy: mechanisms, response biomarkers, and combinations. *Sci. Transl. Med.* **8**, 328rv4 (2016).
- Sharma, P. & Allison, J. P. Immune checkpoint targeting in cancer therapy: toward combination strategies with curative potential. *Cell* **161**, 205–214 (2015).
- Yu, X. et al. The surface protein TIGIT suppresses T cell activation by promoting the generation of mature immunoregulatory dendritic cells. *Nat. Immunol.* **10**, 48–57 (2009).
- Stanietsky, N. et al. The interaction of TIGIT with PVR and PVRL2 inhibits human NK cell cytotoxicity. *Proc. Natl. Acad. Sci. USA* **106**, 17858–17863 (2009).
- Bi, J. et al. T-cell Ig and ITIM domain regulates natural killer cell activation in murine acute viral hepatitis. *Hepatology* **59**, 1715–1725 (2014).
- Bi, J. et al. TIGIT safeguards liver regeneration through regulating natural killer cell–hepatocyte crosstalk. *Hepatology* **60**, 1389–1398 (2014).
- Joller, N. et al. Treg cells expressing the coinhibitory molecule TIGIT selectively inhibit proinflammatory Th1 and Th17 cell responses. *Immunity* **40**, 569–581 (2014).
- Johnston, R. J. et al. The immunoreceptor TIGIT regulates antitumor and antiviral CD8⁺ T cell effector function. *Cancer Cell* **26**, 923–937 (2014).
- Chauvin, J. M. et al. TIGIT and PD-1 impair tumor antigen-specific CD8⁺ T cells in melanoma patients. *J. Clin. Invest.* **125**, 2046–2058 (2015).
- Kong, Y. et al. T-cell immunoglobulin and ITIM domain (TIGIT) associates with CD8⁺ T cell exhaustion and poor clinical outcome in AML patients. *Clin. Cancer Res.* **22**, 3057–3066 (2016).
- Shibuya, A. et al. DNAM-1, a novel adhesion molecule involved in the cytolytic function of T lymphocytes. *Immunity* **4**, 573–581 (1996).
- Chan, C. J. et al. The receptors CD96 and CD226 oppose each other in the regulation of natural killer cell functions. *Nat. Immunol.* **15**, 431–438 (2014).
- Kurtulus, S. et al. TIGIT predominantly regulates the immune response via regulatory T cells. *J. Clin. Invest.* **125**, 4053–4062 (2015).
- van Elsland, A., Hurwitz, A. A. & Allison, J. P. Combination immunotherapy of B16 melanoma using anti-cytotoxic T lymphocyte-associated antigen 4 (CTLA-4) and granulocyte/macrophage colony-stimulating factor (GM-CSF)-producing vaccines induces rejection of subcutaneous and metastatic tumors accompanied by autoimmune depigmentation. *J. Exp. Med.* **190**, 355–366 (1999).
- Yang, Y. F. et al. Enhanced induction of antitumor T-cell responses by cytotoxic T lymphocyte-associated molecule-4 blockade: the effect is manifested only at the restricted tumor-bearing stages. *Cancer Res.* **57**, 4036–4041 (1997).
- Quezada, S. A., Peggs, K. S., Curran, M. A. & Allison, J. P. CTLA4 blockade and GM-CSF combination immunotherapy alters the intratumor balance of effector and regulatory T cells. *J. Clin. Invest.* **116**, 1935–1945 (2006).
- Li, B. et al. Anti-programmed death-1 synergizes with granulocyte macrophage colony-stimulating factor–secreting tumor cell immunotherapy providing therapeutic benefit to mice with established tumors. *Clin. Cancer Res.* **15**, 1623–1634 (2009).
- Curran, M. A. & Allison, J. P. Tumor vaccines expressing flt3 ligand synergize with ctla-4 blockade to reject preimplanted tumors. *Cancer Res.* **69**, 7747–7755 (2009).
- Curran, M. A., Montalvo, W., Yagita, H. & Allison, J. P. PD-1 and CTLA-4 combination blockade expands infiltrating T cells and reduces regulatory T and myeloid cells within B16 melanoma tumors. *Proc. Natl. Acad. Sci. USA* **107**, 4275–4280 (2010).
- Ngiow, S. F. et al. Anti-TIM3 antibody promotes T cell IFN- γ -mediated antitumor immunity and suppresses established tumors. *Cancer Res.* **71**, 3540–3551 (2011).
- Dong, J., McPherson, C. M. & Stambrook, P. J. Flt-3 ligand: a potent dendritic cell stimulator and novel antitumor agent. *Cancer Biol. Ther.* **1**, 486–489 (2002).
- Hou, S. et al. Eradication of hepatoma and colon cancer in mice with Flt3L gene therapy in combination with 5-FU. *Cancer Immunol. Immunother.* **56**, 1605–1613 (2007).
- Salmon, H. et al. Expansion and activation of CD103⁺ dendritic cell progenitors at the tumor site enhances tumor responses to therapeutic PD-L1 and BRAF inhibition. *Immunity* **44**, 924–938 (2016).
- Zou, W. Immunosuppressive networks in the tumour environment and their therapeutic relevance. *Nat. Rev. Cancer* **5**, 263–274 (2005).
- Nagamura-Inoue, T., Mori, Y., Yizhou, Z., Watanabe, N. & Takahashi, T. A. Differential expansion of umbilical cord blood mononuclear cell-derived natural killer cells dependent on the dose of interleukin-15 with Flt3L. *Exp. Hematol.* **32**, 202–209 (2004).
- Lin, S. J., Yang, M. H., Chao, H. C., Kuo, M. L. & Huang, J. L. Effect of interleukin-15 and Flt3-ligand on natural killer cell expansion and activation: umbilical cord vs. adult peripheral blood mononuclear cells. *Pediatr. Allergy Immunol.* **11**, 168–174 (2000).
- Stanietsky, N. et al. Mouse TIGIT inhibits NK-cell cytotoxicity upon interaction with PVR. *Eur. J. Immunol.* **43**, 2138–2150 (2013).
- Gur, C. et al. Binding of the Fap2 protein of *Fusobacterium nucleatum* to human inhibitory receptor TIGIT protects tumors from immune cell attack. *Immunity* **42**, 344–355 (2015).
- Segal, N. H. et al. A phase I dose escalation and cohort expansion study of lirilumab (anti-KIR; BMS-986015) in combination with nivolumab (anti-PD-1; BMS-936558, ONO-4538) in advanced solid tumors. *ASCO Annual Meeting Proc.* **2014**, TPS3115 (2014).
- Zheng, M., Sun, R., Wei, H. & Tian, Z. NK cells help induce anti-hepatitis B virus CD8⁺ T cell immunity in mice. *J. Immunol.* **196**, 4122–4131 (2016).
- Liu, Y. et al. Uncompromised NK cell activation is essential for virus-specific CTL activity during acute influenza virus infection. *Cell. Mol. Immunol.* <https://doi.org/10.1038/cmi.2017.10> (2017).

Acknowledgements

We acknowledged funding support from the following sources: Natural Science Foundation of China (#81788101 to Z.T., #31570893 to R.S., and #81501355 to J.B.); Chinese Academy of Science (XDPB030301 to Z.T.); the Ministry of Science & Technology of China (2017ZX10203206003 to R.S., 2017ZX10202203-002-001 to Y.C.); the Science and Technology Innovation Fund of Shenzhen (JCYJ20150521094519472 and JCYJ20150630114942288 to J.B.). We thank Bristol-Myers Squibb for *Tigit^{-/-}* mice; T. W. Mak (University of Toronto) for the *Nfil3^{+/-}* mice; S. Su (Shantou University) for GKO mice; L. Bai and Z. Lian (University of Science and Technology of China) for C57BL/6J *Cd4^{-/-}* mice; X. Wang (Inner Mongolia University) for *Rag2^{-/-}* mice; E. Vivier (INSERM) for *Ncr1^{Cre/+}* mice; and Z. Fan (Institute of Biophysics, Chinese Academy of Sciences) for *Tigit^{fl/fl}* mice.

Author contributions

Q.Z., R.S. and Z.T. initiated and designed the research; Q.Z. performed all the experiments and analyzed and interpreted results; Q.Z., J.B. and Z.T. wrote the

manuscript; X.Z., Y.C., H.P. and H. Wei contributed to discussions of results; and H. Wang, W.W., Z.W. and Q.W. provided clinical specimens, and clinical and pathological information.

Competing interests

The authors declare no competing interests.

Additional information

Supplementary information is available for this paper at <https://doi.org/10.1038/s41590-018-0132-0>.

Reprints and permissions information is available at www.nature.com/reprints.

Correspondence and requests for materials should be addressed to R.S. or Z.T.

Publisher's note: Springer Nature remains neutral with regard to jurisdictional claims in published maps and institutional affiliations.

Methods

Mice. C57BL/6J, BALB/c, and NOD-SCID mice were purchased from the Shanghai Experimental Animal Center. SCID mice were purchased from Beijing Vital River Company. C57BL/6J *Tigit*^{-/-} mice were obtained from the Bristol-Myers Squibb. C57BL/6J *Nfil3*^{+/-} mice were provided by T. W. Mak (University of Toronto), and *Nfil3*^{-/-} mice were bred in-house. C57BL/6J GKO (IFN- γ -deficient) mice were provided by S. Su (Shantou University). C57BL/6J *Cd4*^{-/-} mice were gifts from L. Bai and Z. Lian (University of Science and Technology of China). C57BL/6J *Ncr1*^{Cre/+} mice were obtained from E. Vivier (INSERM, France). C57BL/6J *Tigit*^{fl/fl} mice were obtained from Z. Fan (Institute of Biophysics, Chinese Academy of Sciences). *Tigit*^{fl/fl}*Ncr1*^{Cre/+} mice were obtained by crossing *Ncr1*^{Cre/+} mice with *Tigit*^{fl/fl} mice. *Rag2*^{-/-} mice were provided by X. Wang (Inner Mongolia University). All mice were maintained in a specific pathogen-free facility for use according to the guidelines for experimental animals at the University of Science and Technology of China. Mice were used between 6 weeks and 8 weeks of age.

Human tumor samples. Fresh colorectal cancer (CRC) tissues were obtained from the First Affiliated Hospital of the Medical University of Anhui (Hefei, China). All specimens were obtained with written informed consent and collected using a protocol approved by the Institutional Review Board of the University of Science and Technology of China. Information on patient with colon cancer is in Supplementary Table 1.

Cell lines and plasmids. CT26.wild-type, B16/F10 (B16) and 4T1 cell lines were purchased from the cell bank of the Chinese Academy of Sciences (Shanghai, China). Hybridoma cells PK136 (anti-NK1.1; in vivo depletion) and TIB210 (anti-CD8⁺ T cells; in vivo depletion) were purchased from ATCC. 13G6 (a blocking monoclonal antibody to mouse TIGIT) was a novel clone generated in-house by ourselves, and no prominent antibody-dependent cell-mediated cytotoxicity was observed in mice (data not shown). All cell lines tested negative for mycoplasma contamination. Mouse *Flt3l* was PCR amplified from bone marrow cells and was inserted into the MCS region of the pLIVE plasmid (Mirus Bio), to construct pLIVE-*mFlt3l*. Firefly luciferase was PCR amplified from pGL3-Basic plasmid (Promega) and was inserted into the pLVTHM plasmid replacing eGFP region, to construct pLVTHM-Luc.

Transplant tumor models and MCA-induced fibrosarcoma. For colon or breast cancer, BALB/c mice were inoculated subcutaneously or intravenously with 5×10^4 CT26.wild-type or 4T1 cells. NOD-SCID, *Rag2*^{-/-} and SCID mice were inoculated subcutaneously at a lower dose of 2×10^4 CT26.wild-type cells. 3 d later, mice were randomized into treatment groups and treated with anti-TIGIT (200 μ g; purified in-house from 13G6 cell supernatants), anti-PD-L1 (200 μ g; 10F.9G2), isotype-matched control antibody (200 μ g; purified in-house from rat μ -serum) or PBS by intraperitoneal injection five times (once every 3 d). For melanoma models, C57BL/6J, *Cd4*^{-/-} or *Nfil3*^{-/-} mice were given hydrodynamic injection of 10 μ g pLIVE-*mFlt3l* or of pLIVE-NULL as a control. 3 d before or after the *Flt3l* injection, mice were inoculated subcutaneously or intravenously with 5×10^4 B16/F10 cells. 3 d after tumor inoculation, mice were treated with anti-TIGIT (200 μ g), isotype-matched control antibody (200 μ g) or PBS by intraperitoneal injection five times (once every 3 d) (antibodies identified above). MCA-induced fibrosarcoma was described as previously²⁵. Mice were given subcutaneous injection of MCA (400 μ g) on the right flank and were monitored over time for the formation of fibrosarcoma. Anti-TIGIT (200 μ g), isotype-matched control antibody (200 μ g) or PBS (antibodies identified above) was injected intraperitoneally on day -1 and day 0 (the day the tumor was injected) and then weekly until week 8. Tumors were measured every day by caliper, and tumor volume was calculated as $0.5 \times \text{length} \times \text{width} \times \text{width}$. Mice were euthanized when tumors grew to larger than 1,000 mm³.

Isolation of TILs. TILs were isolated by dissociating tumor tissue in the presence of collagenase I (0.1% w/v, Sigma) and DNase (0.005% w/v, Sigma) for 1 h before centrifugation on a discontinuous Percoll gradient (GE Healthcare). Isolated cells were then used in various assays of NK cell and T cell function.

Antibodies and flow cytometry. Monoclonal antibodies to mouse NK1.1, mouse CD8 and mouse TIGIT were purified in-house from cell supernatants, and the isotype-matched control antibodies (rat IgG₂) were purified in-house from rat μ serum. Anti-mouse PD-L1 (10F.9G2) for blocking the PD-1–PD-L1 axis in vivo^{37,38} was purchased from Bio X Cell. Rabbit anti-ASGM-1 (986-10001) was purchased from Wako Pure Chemicals. The following reagents were used (all antibodies from BioLegend unless otherwise indicated): annexin V, 7AAD, and FITC-conjugated antibodies to mouse CD3e (145-2C11), CD11b (M1/70), CD69 (H1.2F3) and CD107a (1D4B) (all from BD Bioscience); PE-conjugated antibodies to mice CTLA4 (VC10-4F10-11; BD Bioscience), FasL (MFL3), granzyme B (16G6; eBioscience), IFN- γ (XMG1.2), CD96 (3.3), NKp46 (29A1.4), PD-1 (J43; BD Bioscience), TNF (MP6-XT22), Tim3 (RMT3-23), TRAIL (CD253), CD155

(4.24.1), CD112 (829038; R&D Systems); PerCP-Cy5.5-conjugated antibodies to mouse CD3e (145-2C11), CD8 α (53-6.7), IFN- γ (XMG1.2), NK1.1 (PK136); PerCP-eFluor710 conjugated antibody to mouse TIGIT (GIGD7; eBioscience); PE-Cy7-conjugated antibodies to mouse NKp46 (29A1.4), NK1.1 (PK136) and IFN- γ (XMG1.2); allophycocyanin (APC)-conjugated antibodies to mouse CD8 α (53-6.7), Gr-1 (RB6-8C5), perforin (eBioOMAK-D; eBioscience) and PD-1 (29F.1A12); Alexa Fluor 647-conjugated antibodies to mouse CD226 (10E5) and IFN- γ (XMG1.2); Alexa Fluor 660-conjugated antibody to mouse TIGIT (GIGD7; eBioscience); and APC/Cy7-conjugated antibodies to mouse CD3e (145-2C11) and CD4 (GK1.5). The following antibodies were also used (all from BioLegend unless otherwise indicated): FITC-conjugated antibody to human CD8 (RPA-T8; BD Bioscience), PE-conjugated antibody to human TIGIT (A15153G), PerCP-Cy5.5-conjugated antibody to human CD3 (HIT3a), Alexa-647-conjugated antibody to human CD56 (B159; BD Bioscience) and APC/Cy7-conjugated antibody to human CD45 (2D1). For CD107a and intracellular cytokine staining, splenocytes and TILs cells were stimulated for 4 h with 30 ng/ml phorbol 12-myristate 13-acetate (PMA, Sigma) and 1 μ M ionomycin (Sigma) in the presence of 2.5 μ g/ml monensin (eBioscience). After stimulation, cells were stained for surface markers, fixed and permeabilized with eBioscience FoxP3 fixation buffer according to the manufacturer's instructions. Fixed cells were stained with antibodies to IFN- γ (XMG1.2; BioLegend) and TNF (MP6-XT22, BioLegend). All samples were acquired on an LSR-II or FACSCalibur (BD Biosciences) and were analyzed using FlowJo software (Tree Star).

Cell depletion. For depletion of NK1.1⁺ cells or CD8⁺ T cells, mice were given intraperitoneal injection of 200 μ g mAb to NK1.1 (PK136; purified in-house from cell supernatants) or 200 μ g mAb to CD8 (TIB210; purified in-house from cell supernatants) 24 h before challenge, and after challenge, the antibodies were injected once weekly. For depletion of NK cells in BalB/c mice, anti-ASGM-1^{37,39} was injected intravenously 24 h before challenge, and after challenge, the antibody was injected every 5 d.

Bioluminescence imaging. Bioluminescence imaging and data analysis for photon flux produced by 4T1-Luc metastatic tumors were performed. Mice were given intraperitoneal injection of 20 mg/ml D-luciferin (Gold Biotechnology) at 150 mg per kg body weight 10 min before imaging. Mice were placed into an IVIS imaging chamber (Caliper Life Sciences) when fully anesthetized by isoflurane. Luciferase expression was imaged and calculated by Living Image software.

Immunohistochemistry. Paraffin sections of human tumor tissues were obtained from the First Affiliated Hospital of the Medical University of Anhui (Hefei, China). Slides were de-waxed, rehydrated, subjected to heat-induced epitope retrieval (HIER), and followed by incubation with primary antibodies to human CD155 (81254S, Cell Signaling Technology) and CD112 (AF2229, R&D Systems). The signal was detected using the DAB Peroxidase Substrate Kit (SK-4100) (Vector Laboratories).

Enzyme-linked immunosorbent assay. Flt3L in the serum was measured by ELISA kits according to the manufacturer's instructions (R&D Systems).

Statistical analysis. Statistical analyses were performed in Prism (Graphpad) using appropriate tests as indicated in legends (unpaired two-tailed *t*-test, paired two-tailed *t*-test, one-way ANOVA followed by Tukey's or Dunnett's multiple comparisons test, two-way ANOVA followed by Sidak's multiple comparisons test, multiple *t* test, or the Mantel-Cox test), with significant differences marked on all figures. Significance levels were defined as ns (not significant, $P > 0.05$), * $P < 0.05$, ** $P < 0.01$, *** $P < 0.001$, and **** $P < 0.0001$.

Reporting Summary. Further information on experimental design is available in the Nature Research Reporting Summary linked to this article.

Data availability statement. The datasets generated and/or analyzed during the current study are available from the corresponding author on reasonable request.

References

37. Twyman-Saint Victor, C. et al. Radiation and dual checkpoint blockade activate non-redundant immune mechanisms in cancer. *Nature* **520**, 373–377 (2015).
38. Yang, X. et al. Targeting the tumor microenvironment with interferon- β bridges innate and adaptive immune responses. *Cancer Cell* **25**, 37–48 (2014).
39. Hou, X. et al. CD205-TLR9-IL-12 axis contributes to CpG-induced oversensitive liver injury in HBsAg transgenic mice by promoting the interaction of NK cells with Kupffer cells. *Cell. Mol. Immunol.* **14**, 675–684 (2017).

Reporting Summary

Nature Research wishes to improve the reproducibility of the work that we publish. This form provides structure for consistency and transparency in reporting. For further information on Nature Research policies, see [Authors & Referees](#) and the [Editorial Policy Checklist](#).

Statistical parameters

When statistical analyses are reported, confirm that the following items are present in the relevant location (e.g. figure legend, table legend, main text, or Methods section).

n/a Confirmed

- The exact sample size (n) for each experimental group/condition, given as a discrete number and unit of measurement
- An indication of whether measurements were taken from distinct samples or whether the same sample was measured repeatedly
- The statistical test(s) used AND whether they are one- or two-sided
Only common tests should be described solely by name; describe more complex techniques in the Methods section.
- A description of all covariates tested
- A description of any assumptions or corrections, such as tests of normality and adjustment for multiple comparisons
- A full description of the statistics including central tendency (e.g. means) or other basic estimates (e.g. regression coefficient) AND variation (e.g. standard deviation) or associated estimates of uncertainty (e.g. confidence intervals)
- For null hypothesis testing, the test statistic (e.g. F , t , r) with confidence intervals, effect sizes, degrees of freedom and P value noted
Give P values as exact values whenever suitable.
- For Bayesian analysis, information on the choice of priors and Markov chain Monte Carlo settings
- For hierarchical and complex designs, identification of the appropriate level for tests and full reporting of outcomes
- Estimates of effect sizes (e.g. Cohen's d , Pearson's r), indicating how they were calculated
- Clearly defined error bars
State explicitly what error bars represent (e.g. SD, SE, CI)

Our web collection on [statistics for biologists](#) may be useful.

Software and code

Policy information about [availability of computer code](#)

Data collection

No software was used.

Data analysis

FlowJo 7.6.2 software (Tree Star), Living Image software (PerkinElmer), Graphpad Prism 6.0 (Graphpad).

For manuscripts utilizing custom algorithms or software that are central to the research but not yet described in published literature, software must be made available to editors/reviewers upon request. We strongly encourage code deposition in a community repository (e.g. GitHub). See the Nature Research [guidelines for submitting code & software](#) for further information.

Data

Policy information about [availability of data](#)

All manuscripts must include a [data availability statement](#). This statement should provide the following information, where applicable:

- Accession codes, unique identifiers, or web links for publicly available datasets
- A list of figures that have associated raw data
- A description of any restrictions on data availability

The datasets generated during and/or analysed during the current study are available from the corresponding author on reasonable request.

Field-specific reporting

Please select the best fit for your research. If you are not sure, read the appropriate sections before making your selection.

Life sciences Behavioural & social sciences Ecological, evolutionary & environmental sciences

For a reference copy of the document with all sections, see [nature.com/authors/policies/ReportingSummary-flat.pdf](https://www.nature.com/authors/policies/ReportingSummary-flat.pdf)

Life sciences study design

All studies must disclose on these points even when the disclosure is negative.

Sample size	Sample size was estimated on the basis of similar research reported in the literature (references below). In most of the experiments, 3 to 10 mice/samples was sufficient to identify differences between groups with at least 80% power and a 5% significance level.The number of independent experiment an technical replicates was indicated in each figure legend. Reference: Yu, X. et al. The surface protein TIGIT suppresses T cell activation by promoting the generation of mature immunoregulatory dendritic cells. Nat Immunol10,48-57 (2009). Chan, C.J. et al. The receptors CD96 and CD226 oppose each other in the regulation of natural killer cell functions. Nat Immunol15,431-438 (2014). Johnston, R.J. et al. The immunoreceptor TIGIT regulates antitumor and antiviral CD8(+) T cell effector function. Cancer cell26,923-937 (2014).
Data exclusions	No data were excluded from analyses.
Replication	All experiments were reliably reproduced and every experiment shown was repeated at least three or two times as indicated in the figure legends. We have carefully reported the experimental conditions in the Online Methods and indicated precisely the nature of replicates in Figure legends.
Randomization	Mice were allocated into experimental groups randomly after the injection of tumor cells or MCA.
Blinding	The investigators were not blinded to group allocation during experiments. The experimental observations would be consistent irrespective of blinding. Conclusions were made based on independent experiments, quantitative parameters and statistical significance of the data.

Behavioural & social sciences study design

All studies must disclose on these points even when the disclosure is negative.

Study description	<i>Briefly describe the study type including whether data are quantitative, qualitative, or mixed-methods (e.g. qualitative cross-sectional, quantitative experimental, mixed-methods case study).</i>
Research sample	<i>State the research sample (e.g. Harvard university undergraduates, villagers in rural India) and provide relevant demographic information (e.g. age, sex) and indicate whether the sample is representative. Provide a rationale for the study sample chosen. For studies involving existing datasets, please describe the dataset and source.</i>
Sampling strategy	<i>Describe the sampling procedure (e.g. random, snowball, stratified, convenience). Describe the statistical methods that were used to predetermine sample size OR if no sample-size calculation was performed, describe how sample sizes were chosen and provide a rationale for why these sample sizes are sufficient. For qualitative data, please indicate whether data saturation was considered, and what criteria were used to decide that no further sampling was needed.</i>
Data collection	<i>Provide details about the data collection procedure, including the instruments or devices used to record the data (e.g. pen and paper, computer, eye tracker, video or audio equipment) whether anyone was present besides the participant(s) and the researcher, and whether the researcher was blind to experimental condition and/or the study hypothesis during data collection.</i>
Timing	<i>Indicate the start and stop dates of data collection. If there is a gap between collection periods, state the dates for each sample cohort.</i>
Data exclusions	<i>If no data were excluded from the analyses, state so OR if data were excluded, provide the exact number of exclusions and the rationale behind them, indicating whether exclusion criteria were pre-established.</i>
Non-participation	<i>State how many participants dropped out/declined participation and the reason(s) given OR provide response rate OR state that no participants dropped out/declined participation.</i>
Randomization	<i>If participants were not allocated into experimental groups, state so OR describe how participants were allocated to groups, and if allocation was not random, describe how covariates were controlled.</i>

Ecological, evolutionary & environmental sciences study design

All studies must disclose on these points even when the disclosure is negative.

Study description	Briefly describe the study. For quantitative data include treatment factors and interactions, design structure (e.g. factorial, nested, hierarchical), nature and number of experimental units and replicates.
Research sample	Describe the research sample (e.g. a group of tagged <i>Passer domesticus</i> , all <i>Stenocereus thurberi</i> within Organ Pipe Cactus National Monument), and provide a rationale for the sample choice. When relevant, describe the organism taxa, source, sex, age range and any manipulations. State what population the sample is meant to represent when applicable. For studies involving existing datasets, describe the data and its source.
Sampling strategy	Note the sampling procedure. Describe the statistical methods that were used to predetermine sample size OR if no sample-size calculation was performed, describe how sample sizes were chosen and provide a rationale for why these sample sizes are sufficient.
Data collection	Describe the data collection procedure, including who recorded the data and how.
Timing and spatial scale	Indicate the start and stop dates of data collection, noting the frequency and periodicity of sampling and providing a rationale for these choices. If there is a gap between collection periods, state the dates for each sample cohort. Specify the spatial scale from which the data are taken
Data exclusions	If no data were excluded from the analyses, state so OR if data were excluded, describe the exclusions and the rationale behind them, indicating whether exclusion criteria were pre-established.
Reproducibility	Describe the measures taken to verify the reproducibility of experimental findings. For each experiment, note whether any attempts to repeat the experiment failed OR state that all attempts to repeat the experiment were successful.
Randomization	Describe how samples/organisms/participants were allocated into groups. If allocation was not random, describe how covariates were controlled. If this is not relevant to your study, explain why.
Blinding	Describe the extent of blinding used during data acquisition and analysis. If blinding was not possible, describe why OR explain why blinding was not relevant to your study.
Did the study involve field work?	<input type="checkbox"/> Yes <input type="checkbox"/> No

Field work, collection and transport

Field conditions	Describe the study conditions for field work, providing relevant parameters (e.g. temperature, rainfall).
Location	State the location of the sampling or experiment, providing relevant parameters (e.g. latitude and longitude, elevation, water depth).
Access and import/export	Describe the efforts you have made to access habitats and to collect and import/export your samples in a responsible manner and in compliance with local, national and international laws, noting any permits that were obtained (give the name of the issuing authority, the date of issue, and any identifying information).
Disturbance	Describe any disturbance caused by the study and how it was minimized.

Reporting for specific materials, systems and methods

Materials & experimental systems

n/a	Included in the study
<input type="checkbox"/>	<input checked="" type="checkbox"/> Unique biological materials
<input type="checkbox"/>	<input checked="" type="checkbox"/> Antibodies
<input type="checkbox"/>	<input checked="" type="checkbox"/> Eukaryotic cell lines
<input checked="" type="checkbox"/>	<input type="checkbox"/> Palaeontology
<input type="checkbox"/>	<input checked="" type="checkbox"/> Animals and other organisms
<input checked="" type="checkbox"/>	<input type="checkbox"/> Human research participants

Methods

n/a	Included in the study
<input checked="" type="checkbox"/>	<input type="checkbox"/> ChIP-seq
<input type="checkbox"/>	<input checked="" type="checkbox"/> Flow cytometry
<input checked="" type="checkbox"/>	<input type="checkbox"/> MRI-based neuroimaging

Unique biological materials

Policy information about [availability of materials](#)

Obtaining unique materials All unique material used are readily available from the authors.

Antibodies

Antibodies used

Anti-mouse NK1.1 (pk136), anti-mouse CD8 (TIB210), and anti-mouse TIGIT monoclonal antibodies (13G6) were purified from cell supernatants, and the isotype control antibodies (Rat IgG) were purified from rat serum.
 Anti-mouse PD-L1 (Bio X cell, Catalog Number BE0101, Clone 10F.9G2).
 Rabbit anti-ASGM-1 (Wako Pure Chemicals, Catalog Number 986-10001).
 Annexin-V (BioLegend, Catalog Number 640945).
 7AAD (BioLegend, Catalog Number 420404).
 FITC-conjugated antibodies to mouse CD3 ϵ (Catalog Number 100306, Clone 145-2C11), CD11b (Catalog Number 101206, M1/70), CD69 (Catalog Number 104506, H1.2F3), CD107a (Catalog Number 553793, 1D4B, BD Bioscience). PE-conjugated antibodies to mice CTLA4 (Catalog Number 553720, VC10-4F10-11, BD Bioscience), FasL (Catalog Number 106606, MFL3), Granzyme B (Catalog Number 12-8822, 16G6, eBioscience), IFN- γ (Catalog Number 505808, XMG1.2), CD96 (Catalog Number 131705, 3.3), Nkp46 (Catalog Number 137604, 29A1.4), PD-1 (Catalog Number 551892, J43, BD Bioscience), TNF- α (Catalog Number 506306, MP6-XT22), Tim3 (Catalog Number 119704, RMT3-23), TRAIL (Catalog Number 109306, N2B2), CD155 (Catalog Number 132206, 4.24.1), CD112 (Catalog Number FAB3869P, 829038, R & D). PerCP-Cy5.5-conjugated antibodies to mouse CD3 ϵ (Catalog Number 100328, 145-2C11), CD8 α (Catalog Number 100734, 53-6.7), IFN- γ (Catalog Number 505822, XMG1.2), NK1.1 (Catalog Number 108728, PK136). PerCP-eFluor710 conjugated antibodies to mouse TIGIT (Catalog Number 46-9501-82, GIGD7; eBioscience), PE-Cy7-conjugated antibodies to mouse Nkp46 (Catalog Number 137618, 29A1.4), NK1.1 (Catalog Number 108714, PK136), IFN- γ (Catalog Number 505826, XMG1.2). Allophycocyanin (APC)-conjugated antibodies to mouse CD8 α (Catalog Number 100712, 53-6.7), Gr-1 (Catalog Number 108412, RB6-8C5), perforin (Catalog Number 17-9392-80, eBioOMAK-D; eBioscience), PD-1 (Catalog Number 135210, 29F.1A12). Alexa Fluor 647-conjugated antibodies to mouse CD226 (Catalog Number 128808, 10E5), IFN- γ (Catalog Number 505814, XMG1.2), Alexa Fluor 660-conjugated antibodies to mouse TIGIT (Catalog Number 50-9501-82, GIGD7; eBioscience), APC/Cy7-conjugated antibodies to mouse CD3 ϵ (Catalog Number 100330, 145-2C11), CD4 (Catalog Number 100414, GK1.5). FITC-conjugated antibodies to human CD8 (Catalog Number 368508, 2D1), PE-conjugated antibodies to human TIGIT (Catalog Number 372704, A15153G), PerCP-Cy5.5-conjugated antibodies to human CD3 (Catalog Number 300328, HIT3a), Alexa-647-conjugated antibodies to human CD56 (Catalog Number 557711, B159, BD Bioscience), APC/Cy7-conjugated antibodies to human CD45 (Catalog Number 557833, 2D1, BD Bioscience). Antibodies were all from BioLegend unless otherwise indicated.
 The primary antibodies against human CD155 (Catalog Number 81254S, clone D8A5G, Cell Signaling Technology, U.S.A.) and CD112 (Catalog Number AF2229, R & D).

Validation

Anti-TIGIT mAb (13G6) is purified from 13G6 cells (generated by ourselves) and its validation data are available on Chinese Patent (ZL201210590618.9). All other antibodies are from commercial sources and their validation data are available on the manufacturer's website.

Eukaryotic cell lines

Policy information about [cell lines](#)

Cell line source(s)

CT26.WT, B16/F10 (B16), and 4T1 cell lines were purchased from the cell bank of the Chinese Academy of Sciences (Shanghai, China). Hybridoma cells PK136 (anti-NK1.1 in-vivo depletion) and TIB210 (anti-CD8+T, in-vivo depletion) were purchased from ATCC. 13G6 (a blocking anti-mouse TIGIT monoclonal antibody) was a novel clone generated in mouse by ourselves.

Authentication

Authentication was performed by ATCC for CT26.WT, B16/F10, 4T1, PK136 and TIB210 cell line (Method: STR profiling). Authentication was performed by us for 13G6 cell line (methods: FACS, ELISA, Western Blot et. referring to Chinese patent ZL201210590618.9)

Mycoplasma contamination

All cell lines tested negative for mycoplasma contamination.

Commonly misidentified lines
(See [ICLAC](#) register)

No commonly misidentified cell lines were used.

Palaeontology

Specimen provenance

Provide provenance information for specimens and describe permits that were obtained for the work (including the name of the issuing authority, the date of issue, and any identifying information).

Specimen deposition

Indicate where the specimens have been deposited to permit free access by other researchers.

Dating methods

If new dates are provided, describe how they were obtained (e.g. collection, storage, sample pretreatment and measurement), where they were obtained (i.e. lab name), the calibration program and the protocol for quality assurance OR state that no new dates are provided.

Tick this box to confirm that the raw and calibrated dates are available in the paper or in Supplementary Information.

Animals and other organisms

Policy information about [studies involving animals](#); [ARRIVE guidelines](#) recommended for reporting animal research

Laboratory animals

C57BL/6 J, BALB/c, and NOD-SCID mice were purchased from the Shanghai Experimental Animal Center (Shanghai, China). SCID mice were purchased from Beijing Vital River Company (Beijing, China). C57BL/6 J Tigit^{-/-} mice were obtained from the Bristol-Myers Squibb Company (New York, NY, U.S.A.). C57BL/6 J Nfil3^{+/-} mice were provided by Dr. Tak W. Mak (University of Toronto, Toronto, Ontario, Canada), and Nfil3^{-/-} mice were bred in-house. C57BL/6 J GKO (IFN- γ -deficient) mice were provided by Dr. Shaobo Su (Shantou University, Shantou, China). C57BL/6 J Cd4^{-/-} mice were kind gifts from Dr. Li Bai and Dr. Zhexiong Lian (University of Science and Technology of China, Hefei, China). C57BL/6 J Ncr1iCre/+ mice were obtained from Dr. Eric Vivier (INSERM, France). C57BL/6 J Tigitfl/fl mice were obtained from Dr. Zusen Fan (Institute of Biophysics, Chinese Academy of Sciences, China). Tigitfl/fl- Ncr1iCre/+ mice were obtained by crossing Ncr1iCre/+ mice with Tigitfl/fl mice. Rag2^{-/-} mice were kindly provided by Dr. Xin Wang (Inner Mongolia University, Hohhot, China). All mice were maintained in a specific pathogen-free facility for use according to the guidelines for experimental animals at the University of Science and Technology of China. Male mice were used between 6-8 weeks of age.

Wild animals

The study did not involve wild animals.

Field-collected samples

The study did not involve samples collected from the field.

Human research participants

Policy information about [studies involving human research participants](#)

Population characteristics

Describe the covariate-relevant population characteristics of the human research participants (e.g. age, gender, genotypic information, past and current diagnosis and treatment categories). If you filled out the behavioural & social sciences study design questions and have nothing to add here, write "See above."

Recruitment

Describe how participants were recruited. Outline any potential self-selection bias or other biases that may be present and how these are likely to impact results.

ChIP-seq

Data deposition

Confirm that both raw and final processed data have been deposited in a public database such as [GEO](#).

Confirm that you have deposited or provided access to graph files (e.g. BED files) for the called peaks.

Data access links

May remain private before publication.

For "Initial submission" or "Revised version" documents, provide reviewer access links. For your "Final submission" document, provide a link to the deposited data.

Files in database submission

Provide a list of all files available in the database submission.

Genome browser session

(e.g. [UCSC](#))

Provide a link to an anonymized genome browser session for "Initial submission" and "Revised version" documents only, to enable peer review. Write "no longer applicable" for "Final submission" documents.

Methodology

Replicates

Describe the experimental replicates, specifying number, type and replicate agreement.

Sequencing depth

Describe the sequencing depth for each experiment, providing the total number of reads, uniquely mapped reads, length of reads and whether they were paired- or single-end.

Antibodies

Describe the antibodies used for the ChIP-seq experiments; as applicable, provide supplier name, catalog number, clone name, and lot number.

Peak calling parameters

Specify the command line program and parameters used for read mapping and peak calling, including the ChIP, control and index files used.

Data quality

Describe the methods used to ensure data quality in full detail, including how many peaks are at FDR 5% and above 5-fold enrichment.

Software

Describe the software used to collect and analyze the ChIP-seq data. For custom code that has been deposited into a community repository, provide accession details.

Flow Cytometry

Plots

Confirm that:

- The axis labels state the marker and fluorochrome used (e.g. CD4-FITC).
- The axis scales are clearly visible. Include numbers along axes only for bottom left plot of group (a 'group' is an analysis of identical markers).
- All plots are contour plots with outliers or pseudocolor plots.
- A numerical value for number of cells or percentage (with statistics) is provided.

Methodology

Sample preparation	Tumor was cut into small pieces, followed by treatment with collagenase I (0.1% w/v, Sigma) and DNase (0.005% w/v, Sigma) in DMEM (1 h at RT, 220 rpm). Lung was cut into small pieces, followed by treatment with collagenase I (0.1% w/v, Sigma) in DMEM (1h at RT, 220 rpm). Liver was homogenized through a 70 micron filter in PBS. Single cell suspensions of tumor, lung and lung were purified on a 40%/70% Percoll gradient (800 g at 23°C for 30 min). Spleen was homogenized through a 70 micron filter in PBS, and single cell suspensions of splenocytes were treated with ACK Lysis buffer to lyse RBC.
Instrument	LSR-II or FACS-Calibur (BD Biosciences).
Software	BD FACS DIVA was used for collection and analysis was done in FlowJo7.6.2.
Cell population abundance	e Not applicable.
Gating strategy	Starting cells were gated by FSC/SSC gates. These cells were further gated by CD45 for leukocytes. Next, CD3-NK1.1+, CD3-NKp46+, CD3+CD8+, or CD3+CD4+ cells were analyzed in CD45+ gate.

- Tick this box to confirm that a figure exemplifying the gating strategy is provided in the Supplementary Information.

Magnetic resonance imaging

Experimental design

Design type	<i>Indicate task or resting state; event-related or block design.</i>
Design specifications	<i>Specify the number of blocks, trials or experimental units per session and/or subject, and specify the length of each trial or block (if trials are blocked) and interval between trials.</i>
Behavioral performance measures	<i>State number and/or type of variables recorded (e.g. correct button press, response time) and what statistics were used to establish that the subjects were performing the task as expected (e.g. mean, range, and/or standard deviation across subjects).</i>

Acquisition

Imaging type(s)	<i>Specify: functional, structural, diffusion, perfusion.</i>
Field strength	<i>Specify in Tesla</i>
Sequence & imaging parameters	<i>Specify the pulse sequence type (gradient echo, spin echo, etc.), imaging type (EPI, spiral, etc.), field of view, matrix size, slice thickness, orientation and TE/TR/flip angle.</i>
Area of acquisition	<i>State whether a whole brain scan was used OR define the area of acquisition, describing how the region was determined.</i>
Diffusion MRI	<input type="checkbox"/> Used <input type="checkbox"/> Not used

Preprocessing

Preprocessing software	<i>Provide detail on software version and revision number and on specific parameters (model/functions, brain extraction, segmentation, smoothing kernel size, etc.).</i>
Normalization	<i>If data were normalized/standardized, describe the approach(es): specify linear or non-linear and define image types used for transformation OR indicate that data were not normalized and explain rationale for lack of normalization.</i>
Normalization template	<i>Describe the template used for normalization/transformation, specifying subject space or group standardized space (e.g. original Talairach, MNI305, ICBM152) OR indicate that the data were not normalized.</i>
Noise and artifact removal	<i>Describe your procedure(s) for artifact and structured noise removal, specifying motion parameters, tissue signals and physiological signals (heart rate, respiration).</i>

Volume censoring

*Define your software and/or method and criteria for volume censoring, and state the extent of such censoring.***Statistical modeling & inference**

Model type and settings

Specify type (mass univariate, multivariate, RSA, predictive, etc.) and describe essential details of the model at the first and second levels (e.g. fixed, random or mixed effects; drift or auto-correlation).

Effect(s) tested

*Define precise effect in terms of the task or stimulus conditions instead of psychological concepts and indicate whether ANOVA or factorial designs were used.*Specify type of analysis: Whole brain ROI-based BothStatistic type for inference
(See [Eklund et al. 2016](#))*Specify voxel-wise or cluster-wise and report all relevant parameters for cluster-wise methods.*

Correction

*Describe the type of correction and how it is obtained for multiple comparisons (e.g. FWE, FDR, permutation or Monte Carlo).***Models & analysis**

n/a | Involved in the study

 Functional and/or effective connectivity Graph analysis Multivariate modeling or predictive analysis

Functional and/or effective connectivity

Report the measures of dependence used and the model details (e.g. Pearson correlation, partial correlation, mutual information).

Graph analysis

Report the dependent variable and connectivity measure, specifying weighted graph or binarized graph, subject- or group-level, and the global and/or node summaries used (e.g. clustering coefficient, efficiency, etc.).

Multivariate modeling and predictive analysis

Specify independent variables, features extraction and dimension reduction, model, training and evaluation metrics.